

ARTICLE

Inhibition of CRTH2-mediated Th2 activation attenuates pulmonary hypertension in mice

Guilin Chen¹, Shengkai Zuo¹, Juan Tang², Caojian Zuo³, Daile Jia³, Qian Liu², Guizhu Liu² , Qian Zhu³, Yuanyang Wang^{1,2}, Jian Zhang^{1,2}, Yujun Shen^{1,2} , Dongrui Chen⁴, Ping Yuan⁵, Zhiqiang Qin⁶, Chengchao Ruan⁴, Jue Ye⁷, Xiao-jian Wang⁷, Yuping Zhou⁷, Pingjin Gao⁴, Peng Zhang⁵, Jinming Liu⁵, Zhi-Cheng Jing⁸ , Ankang Lu³, and Ying Yu^{1,2} 

Pulmonary arterial hypertension (PAH) is a life-threatening disease characterized by progressive pulmonary artery (PA) remodeling. T helper 2 cell (Th2) immune response is involved in PA remodeling during PAH progression. Here, we found that CRTH2 (chemoattractant receptor homologous molecule expressed on Th2 cell) expression was up-regulated in circulating CD3⁺CD4⁺ T cells in patients with idiopathic PAH and in rodent PAH models. CRTH2 disruption dramatically ameliorated PA remodeling and pulmonary hypertension in different PAH mouse models. CRTH2 deficiency suppressed Th2 activation, including IL-4 and IL-13 secretion. Both CRTH2^{+/+} bone marrow reconstitution and CRTH2^{+/+} CD4⁺ T cell adoptive transfer deteriorated hypoxia + ovalbumin-induced PAH in CRTH2^{-/-} mice, which was reversed by dual neutralization of IL-4 and IL-13. CRTH2 inhibition alleviated established PAH in mice by repressing Th2 activity. In culture, CRTH2 activation in Th2 cells promoted pulmonary arterial smooth muscle cell proliferation through activation of STAT6. These results demonstrate the critical role of CRTH2-mediated Th2 response in PAH pathogenesis and highlight the CRTH2 receptor as a potential therapeutic target for PAH.

Introduction

Pulmonary arterial hypertension (PAH) is a pathophysiological disorder characterized by remodeling of the pulmonary arteries (PAs), resulting in a progressive increase in pulmonary vascular resistance, right ventricular (RV) hypertrophy, and ultimately right heart failure (Galiè et al., 2016). Although significant progress has been made in the treatment of PAH in the past several decades, current pharmacological approaches such as endothelin receptor antagonists, vasodilators, and phosphodiesterase inhibitors provide mainly symptomatic relief with few improvements in overall survival (Rabinovitch, 2012). As a severe and debilitating lung disease, PAH still contributes to unacceptably high morbidity and mortality of patients with cardiopulmonary diseases (Benza et al., 2010). Therefore, identifying new molecules or signaling pathways triggering or mediating PA remodeling, which may serve as potential therapeutic targets, is urgently needed.

Pulmonary arterial smooth muscle cell (SMC [PASMC]) proliferation and hypertrophy and extracellular matrix deposition

contribute to medial hypertrophy and muscularization, leading to narrowness or obstruction of PAs and sustained elevation of pulmonary arterial pressure (Rabinovitch, 2012). Emerging studies demonstrated that perivascular immune and inflammatory responses play an essential role in the pathogenesis of idiopathic PAH (Savai et al., 2012; Stacher et al., 2012; Yeager et al., 2012). Moreover, elevated serum levels of multiple inflammatory cytokines and chemokines are also observed in patients with PAH (Anwar et al., 2016). Of note, marked infiltration of CD4⁺ T cells is observed around PAs in patients with PAH (Savai et al., 2012). In experimental PAH animal models, different soluble antigens such as *Aspergillus fumigatus* and OVA could induce severe muscularization in PAs and PAH by triggering CD4⁺ T helper 2 (Th2) response (Daley et al., 2008). In addition, Th2 cytokines, IL-4 and IL-13, are involved in the development of PAH in multiple PAH animal models (Park et al., 2014; Yamaji-Kegan et al., 2014; Kumar et al., 2015). These observations suggest that Th2-mediated

¹Department of Pharmacology, Key Laboratory of Immune Microenvironment and Disease (Ministry of Education), School of Basic Medical Sciences, Tianjin Medical University, Tianjin, China; ²Institute for Nutritional Sciences, Shanghai Institutes for Biological Sciences, University of Chinese Academy of Sciences, Shanghai, China; ³Department of Cardiology, Ruijin Hospital, Shanghai Jiaotong University School of Medicine, Shanghai, China; ⁴Shanghai Institute of Hypertension, Shanghai Jiao Tong University School of Medicine, Shanghai, China; ⁵Department of Cardio-Pulmonary Circulation, Shanghai Pulmonary Hospital, Tongji University School of Medicine, Shanghai, China; ⁶National Institute of Parasitic Diseases, Chinese Center for Disease Control and Prevention, Shanghai, China; ⁷Thrombosis and Vascular Medicine Center, State Key Laboratory of Cardiovascular Disease, Fu Wai Hospital, National Center for Cardiovascular Disease, Chinese Academy of Medical Sciences and Peking Union Medical College, Beijing, China; ⁸Key Laboratory of Pulmonary Vascular Medicine, Peking Union Medical College and Chinese Academy of Medical Sciences, Beijing, China.

Correspondence to Ying Yu: yuying@tmu.edu.cn.

© 2018 Tianjin Medical University This article is distributed under the terms of an Attribution–Noncommercial–Share Alike–No Mirror Sites license for the first six months after the publication date (see <http://www.rupress.org/terms/>). After six months it is available under a Creative Commons License (Attribution–Noncommercial–Share Alike 4.0 International license, as described at <https://creativecommons.org/licenses/by-nc-sa/4.0/>).

immune reaction is implicated in the pathogenesis of PAH and may be used as an intervention option for PAH therapy.

G protein-coupled receptor 44 (GPR44) structurally belongs to the family of chemoattractant receptors (Marchese et al., 1999). It is selectively expressed in Th2 lineage cells and, thus, is named chemoattractant receptor homologous molecule expressed on Th2 (CRTH2; Nagata et al., 1999b). Prostaglandin (PG) D₂ is a natural ligand for CRTH2 receptor; its activation can induce intracellular Ca²⁺ mobilization and chemotaxis in Th2 cells in a G_{ai}-dependent fashion (Hirai et al., 2001). Moreover, PGD₂ preferentially elicits the secretion of proinflammatory cytokines such as IL-4, IL-5, and IL-13 in Th2 cells in a dose-dependent manner through CRTH2 (Xue et al., 2005). Additionally, immunoglobulin E-stimulated mast cells invoke IL-4 and IL-13 production by Th2 cells through interaction of PGD₂ and CRTH2 on Th2 cells (Xue et al., 2009). Therefore, activation of CRTH2 increases pulmonary allergic inflammation in mice and humans (Spik et al., 2005; Schmidt et al., 2013; Palikhe et al., 2016). However, whether CRTH2-mediated Th2 cell activation contributes to the development of PAH remains unclear.

In this study, we demonstrated that CRTH2 expression in circulating CD4⁺ T cells and serum Th2 cytokines was elevated in patients with PAH and in PAH mouse models. CRTH2 deficiency attenuated the development of hypoxia-induced PAH in mice by suppression of Th2 immune responses in the lungs. CRTH2^{+/-} bone marrow (BM) transplantation (BMT) or CRTH2^{+/-} T cell adoptive transfer augmented hypoxia + OVA (HyOA)-induced PAH in CRTH2^{-/-} mice, which was ameliorated by neutralization of both IL-4 and IL-13. Inhibition of CRTH2 alleviated HyOA-induced PAH in mice. Mechanistically, Th2 cell-derived IL-4 and IL-13 promoted PASMC proliferation by activation of STAT6. These results demonstrated that CRTH2-mediated Th2 activation is implicated in the pathogenesis of PAH.

Results

Enhanced Th2 immune response in patients with PAH and in mice exposed to chronic hypoxia

Inflammation and autoimmunity play an important role in the development of PAH (Kherbeck et al., 2013). To investigate whether T cell activation is involved in the pathogenesis of PAH, we analyzed alterations of T cell subpopulations, their cytokine levels, and other related inflammatory cells in the plasma from patients with idiopathic PAH. Peripheral blood mononuclear cells (PBMCs) from patients with PAH and age-matched healthy subjects were collected, and the subpopulations and frequencies of T cells were determined by using flow cytometry. We observed that the proportion, total number ($[5.9 \pm 0.2] \times 10^3/\text{ml}$ vs. $[1.1 \pm 0.1] \times 10^3/\text{ml}$, $P < 0.05$) of Th cells (CD3⁺CD4⁺ cells) in PBMCs from patients with PAH were markedly increased compared with those in PBMCs from healthy subjects (Table 1). The cytotoxic T cell ratio (CD3⁺CD8⁺ cells) was not significantly changed (Table 1), whereas total CD3⁺CD8⁺ T cells were elevated ($[2.8 \pm 0.2] \times 10^3/\text{ml}$ vs. $[0.7 \pm 0.1] \times 10^3/\text{ml}$, $P < 0.05$). The relative expression of GATA3 and Th2 cytokines (IL-4, IL-5, and IL-13) was strikingly up-regulated in plasma CD4⁺ T cells isolated from patients with PAH (Table 1). No significant change was observed

for the other transcriptional factors (such as GATA2, Tbx21, and RORC; Table 1) and cytokines tested (such as IFN- γ , TNF- α , and IL-1 β ; unpublished data). Moreover, secretion of Th2 cytokines and periostin (Table 1) in the peripheral blood from patients with PAH was significantly increased compared with that observed in healthy subjects (Table 1). Accordingly, the populations of Th2 main effect cells such as eosinophils, mast cells, and IgE-producing B cells were increased in peripheral blood in PAH patients. In contrast, T reg cell proportion and Foxp3 expression were markedly decreased in peripheral blood in PAH patients (Table 1). Similarly, marked elevation of eosinophils, mast cells, basophils, and IgE-producing B cells in peripheral blood, bronchoalveolar lavage fluid (BALF), and lung tissues was detected in HyOA-induced PAH in mice (Fig. S1, A-F). Interestingly, the frequency of CD3⁺CD4⁺ T cells in circulation (not depicted) and lung tissues of hypoxia-challenged mice were also increased as compared with that from control mice (Fig. 1, A and B). Again, expression of Th2 cytokines (IL-4, IL-5, and IL-13) was markedly up-regulated in lung CD4⁺ T cells from hypoxia-challenged mice (Fig. 1 C), and secretion of these cytokines in the BALF was significantly increased in hypoxia-challenged mice (Fig. 1 D). Thus, the results indicated that Th2 immune response is exaggerated during the progression of PAH.

Expression of CRTH2 is up-regulated in CD4⁺ T cells isolated from patients with PAH and mouse PAH models

PG is an important lipid mediator of inflammation. Thus, we examined the mRNA expression of all PG receptors (I-prostanoid receptor [IP], E-prostanoid receptor subtypes 1-4 [EP1-EP4], D-prostanoid receptor 1 [DP1], CRTH2, thromboxane-prostanoid receptor [TP], and PG F₂ receptor [FP]) in isolated CD4⁺ T cells from patients with PAH and mouse PAH models. Of these receptors, CRTH2 mRNA levels were increased in CD4⁺ T cells from patients with PAH compared with those from healthy subjects (Fig. 1 E), which was confirmed by flow cytometry analysis (Fig. 1, F and G). Elevated expression of Crth2 was also observed in CD4⁺ T cells in the lungs from hypoxia-treated mice (Fig. 1 H). Moreover, hematopoietic PG D synthase (H-PGDS) expression in CD4⁺ T cells and PGD₂ product in lung tissues from chronic hypoxia-challenged mice were also markedly increased compared with those in lung tissues from control mice (Fig. 1, H and I).

CRTH2 deficiency ameliorates PA pressure and pulmonary arterial remodeling by suppressing Th2 response in mouse models induced by hypoxia + SU5416 (HySU)

Given the elevated expression of CRTH2 in circulating CD4⁺ T cells in patients with PAH and lung tissues of hypoxia-induced PAH mouse models, we tested whether CRTH2 deletion would influence the progression of PAH. After a 3-wk exposure to chronic hypoxia (10% O₂) with administration of SU5416 (an angiogenesis inhibitor; Fig. 2 A), mice developed a significant elevation in RV systolic pressure (RVSP; Fig. 2 B) and in the ratio of the weight of the free RV wall to the weight of the left ventricular (LV) wall plus the septum (RV/LV + S; Fig. 2 C) compared with that observed in control mice. Intriguingly, CRTH2-deficient (CRTH2^{-/-}) mice displayed a significant reduction in RVSP (29.4 ± 0.9 mm Hg vs. 37.8 ± 2.3 mm Hg, $P < 0.05$; Fig. 2 B) and in RV/

Table 1. Characteristics of iPAH patients

Parameter	iPAH patients (n = 32)	Healthy subjects (n = 25)	P
General characteristics			
Male/female (number)	14/18	12/13	0.75
Age (yr)	33.3 ± 1.4	34.6 ± 2.2	0.73
BMI (kg/m ²)	23.0 ± 0.8	23.2 ± 0.5	0.81
Heart rate (beats per min)	82.4 ± 2.1	79.3 ± 2.4	0.34
6MWD (m)	439.6 ± 19.1	—	—
mPAP (mm Hg)	54.9 ± 3.5	—	—
PCWP (mm Hg)	9.5 ± 0.6	—	—
CO (L/min)	4.8 ± 0.4	—	—
PVR (WU)	11.2 ± 1.2	—	—
mRAP (mm Hg)	9.8 ± 0.9	—	—
Proteins^a			
IL-4 (pg/ml)	309.1 ± 22.9	168.2 ± 16.9	<0.01
IL-5 (pg/ml)	213.1 ± 13.7	116.6 ± 8.6	<0.01
IL-13 (pg/ml)	255.2 ± 17.3	103.7 ± 11.9	<0.01
Periostin (ng/ml)	54.0 ± 1.2	33.6 ± 1.3	<0.01
IgE (ng/ml)	205.6 ± 11.1	63.2 ± 11.9	<0.01
Blood cells (%)^b			
CD4 ⁺ cells	31.2 ± 1.7	18.9 ± 0.9	<0.01
CD8 ⁺ cells	15.2 ± 1.1	13.8 ± 0.7	0.26
CD4/CD8	2.1 ± 0.2	1.4 ± 0.1	<0.01
Eosinophil	3.3 ± 0.3	2.0 ± 0.2	<0.01
Basophil	8.4 ± 1.0	6.1 ± 0.6	0.08
Mast	0.2 ± 0.0	0.1 ± 0.0	<0.01
ILC2	1.2 ± 0.1	1.0 ± 0.1	0.12
B cell	3.5 ± 0.4	1.7 ± 0.2	<0.01
T reg	2.7 ± 0.4	6.6 ± 0.6	<0.01
Gene expression (q-PCR)^c			
Tbx21	(1.7 ± 0.2) × 10 ⁻³	(1.4 ± 0.3) × 10 ⁻³	0.48
GATA2	(2.4 ± 0.2) × 10 ⁻³	(2.0 ± 0.1) × 10 ⁻³	0.22
GATA3	(1.6 ± 0.1) × 10 ⁻²	(0.7 ± 0.1) × 10 ⁻²	<0.01
RORC	(2.5 ± 0.3) × 10 ⁻³	(2.3 ± 0.3) × 10 ⁻³	0.60
Foxp3	(1.5 ± 0.2) × 10 ⁻³	(2.7 ± 0.4) × 10 ⁻³	<0.01
IL-4	0.27 ± 0.09	0.02 ± 0.01	<0.01
IL-5	0.21 ± 0.06	0.07 ± 0.01	<0.01
IL-13	0.28 ± 0.05	0.02 ± 0.01	<0.01
IFN-γ	0.22 ± 0.06	0.19 ± 0.04	0.65
TNF-α	0.09 ± 0.01	0.08 ± 0.01	0.73
IL-1β	0.03 ± 0.01	0.03 ± 0.01	0.72

Values are presented as means ± SEMs. 6MWD, 6-min walking distance; BMI, body mass index; iPAH, idiopathic PAH; mPAP, mean pulmonary arterial pressure; CO, cardiac output; mRAP, mean right atrial pressure; PCWP, pulmonary capillary wedge pressure; PVR, pulmonary vascular resistance; WU, Woods units.

^aLevels of serum cytokines and IgE in human subjects were evaluated by ELISA. For iPAH patients, n = 25; for healthy subjects, n = 18.

^bInflammatory cells in peripheral blood of human subjects were analyzed by flow cytometry. For iPAH patients, n = 6–7; for healthy subjects, n = 6–8.

^cGene expression in human CD4⁺ T cells was determined by quantitative PCR (q-PCR). For iPAH patients, n = 6; for healthy subjects, n = 6.

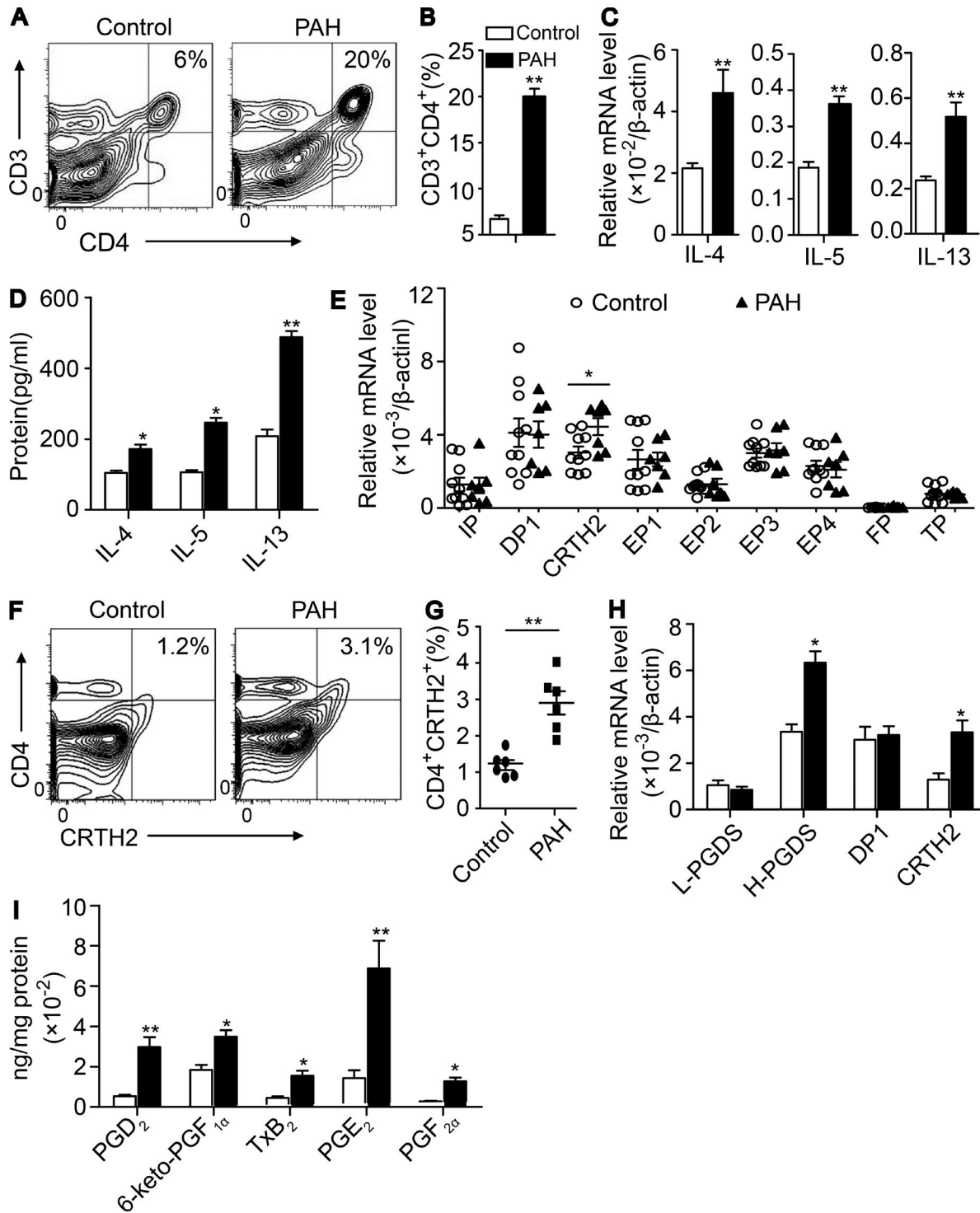


Figure 1. Circulating Th2 cells and CRTH2 expression in T cells are increased in patients with idiopathic PAH and mice exposed to hypoxia. (A–D) Activated Th2 response in lung tissues of chronic hypoxia-challenged mice. (A) Flow cytometric analysis of CD3⁺CD4⁺ T cells in lung tissues. (B) Quantification of the frequency of CD3⁺CD4⁺ T cells in lung tissues. (C) Relative mRNA expression of IL-4, IL-5, and IL-13 in CD4⁺ T cells in lung tissues. (D) Quantification of the frequency of IL-4, IL-5, and IL-13 protein levels in BALF by ELISA. In A–D, *n* = 6–8 mice per group. *, *P* < 0.05; **, *P* < 0.01 versus normoxia group. (E) Relative mRNA levels of PG receptors in isolated CD4⁺ T cells from patients with PAH and healthy subjects. Patients, *n* = 7; healthy subjects, *n* = 10. *, *P* < 0.05 versus healthy subjects. (F) CRTH2 expression in CD4⁺ T cells from patients with PAH and healthy subjects by flow cytometry. (G) Quantification of the frequency of CD4⁺CRTH2⁺ T cells in white blood cells from patients with PAH and healthy subjects. Patients, *n* = 6; healthy subjects, *n* = 6. **, *P* < 0.01 versus healthy subjects. (H) Relative mRNA levels of L-PGDS, H-PGDS, and PGD₂ receptors (DP1 and CRTH2) in CD4⁺ T cells isolated from lung tissues of mice exposed to chronic hypoxia. L-PGDS = lipocalin-type PGD₂ synthase; H-PGDS = hematopoietic PGD₂ synthase. (I) PG production in the lung tissues of hypoxia-challenged mice analyzed by LC-MS. In H and I, *n* = 6–8 mice per group. *, *P* < 0.05; **, *P* < 0.01 versus normoxia group. All graphs are shown as mean ± SEM. Data are representative of at least two independent experiments. Statistical significance was determined using unpaired Student's *t* tests. PGF_{2α}, prostaglandin F_{2α}; TxB₂, thromboxane B₂; PGE₂, prostaglandin E₂.

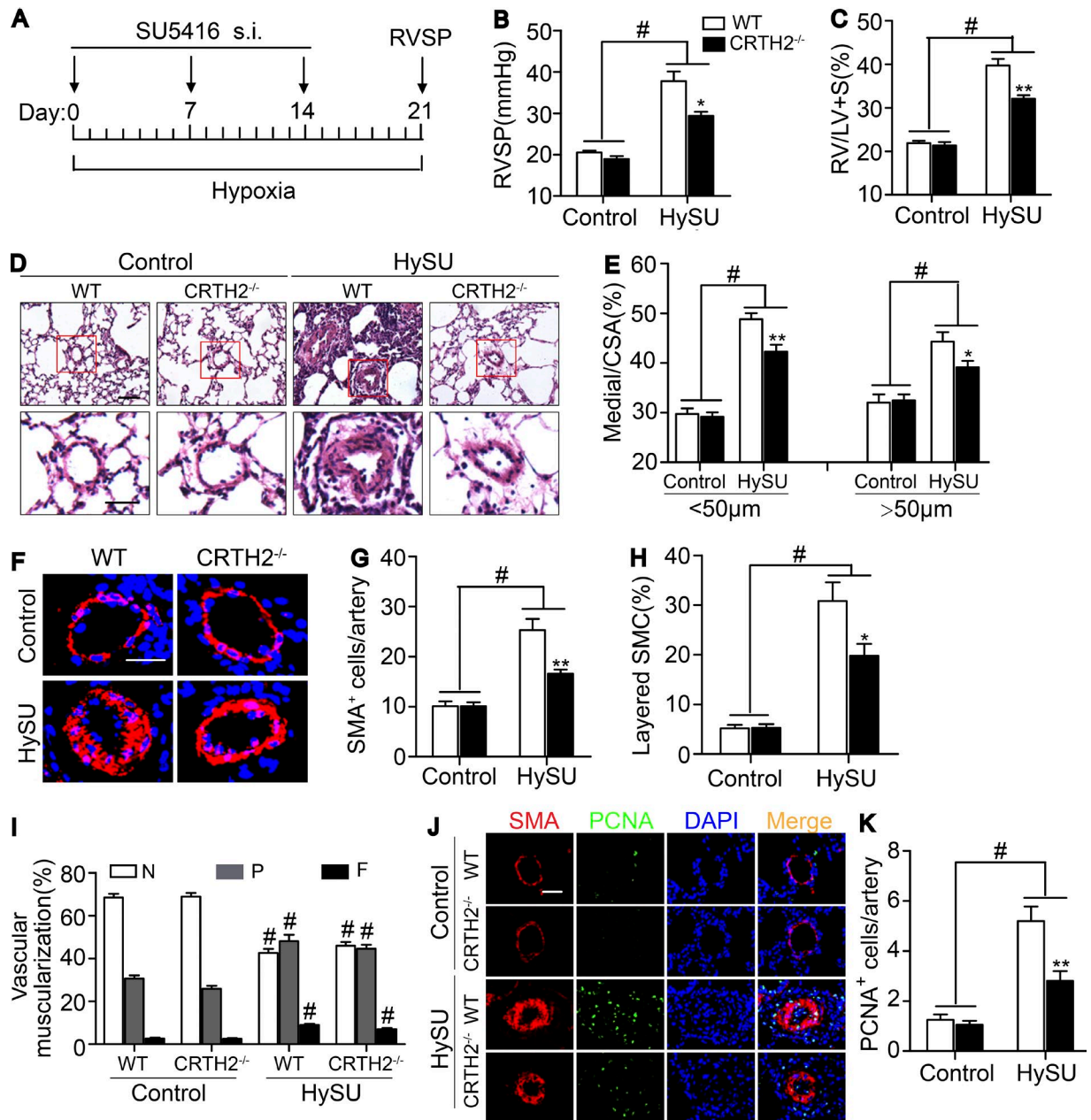


Figure 2. The absence of CRTH2 attenuates the development of chronic HySU-induced PAH in mice. (A) Protocol for HySU-induced PAH in mice. (B) RVSP in CRTH2^{-/-} and WT mice after HySU treatment. (C) Fulton index (RV/LV + S) in CRTH2^{-/-} and WT mice after HySU 6 treatment. (D) Representative images of H&E staining of lung sections from HySU-treated CRTH2^{-/-} and WT mice. Bar, 20 µm. (E) Quantification of the ratio of pulmonary arterial medial thickness to total vessel size (media/CSA) for the HySU treatment models. (F) α-SMA immunostaining of lung sections from HySU-treated CRTH2^{-/-} and WT mice and controls. Bar, 20 µm. (G) Quantification of the number of SMCs in PAs from mice treated with HySU. (H) Quantification of the percent layered SMCs in PAs. (I) Proportion of nonmuscularized (N), partially muscularized (P), or full muscularized (F) pulmonary arterioles (20–50 µm in diameter) from HySU-treated and control mice. (J) Representative images of PCNA and α-SMA immunostaining of the lung tissues from HySU-challenged WT and CRTH2^{-/-} mice. Bar, 20 µm. (K) Quantification of PCNA-expressing cells in PAs. In A–K, n = 8–10 mice per group. *, P < 0.05; **, P < 0.01 versus WT; and #, P < 0.05 versus control. All graphs are shown as mean ± SEM. Data are representative of at least two independent experiments. Statistical analysis was performed using two-way ANOVA followed by a Bonferroni post hoc test and unpaired Student’s t tests.

LV + S (32.1 ± 0.8% vs. 39.7 ± 1.5%, P < 0.01; Fig. 2 C). Meanwhile, expression of hypoxia-inducible factor 1α (HIF-1α) in lung tissues was examined to further validate hypoxia treatment (Fig. S2 A). Moreover, CRTH2 deletion attenuated pulmonary vascular remodeling induced by HySU and reduced vascular wall thickness as a result of decreased media (Fig. 2, D and E), with a significant decrease in α-smooth muscle actin (α-SMA)-expressing

cells and remarkable changes in the organization of SMCs (Fig. 2, F–H), resulting in an improvement of pulmonary vascular muscularization (Fig. 2 I). CRTH2 deficiency inhibited the excessive proliferation of α-SMA-positive cells (Fig. 2, J and K). However, we failed to observe notable differences in intimal thickness, deposition of extracellular matrix, and size of PASMCs of pulmonary vessels between WT and CRTH2^{-/-} mice (Fig. S2, B–F).

As expected, the infiltrated CD4⁺ T cells around PAs in the lungs of CRTH2^{-/-} mice were dramatically reduced (Fig. 3, A and B), and the percentage (Fig. 3, C and D) and total number (Fig. 3 E) of Th2 cells (CD4⁺IL-4⁺ cells) in lung tissues were significantly reduced in HySU-treated CRTH2^{-/-} mice as compared with that in HySU-treated WT mice. There were no significant differences in perivascular infiltration of macrophages (CD68⁺ or Mac-3⁺ cells) and neutrophils (Ly6G⁺ cells) in lung tissues of WT and CRTH2^{-/-} mice (Fig. S2, G–L). Accordingly, levels of IL-4, IL-5, and IL-13, the main cytokines secreted by Th2 cells, were notably inhibited in both the serum (Fig. 3 F) and BALF (Fig. 3 G) from CRTH2^{-/-} mice after HySU challenge compared with those in WT mice. Moreover, CRTH2 deletion strikingly reduced the transcription levels of IL-4 and IL-13 (unpublished data) in the lungs after HySU treatment. However, we did not detect significant alterations of the expression of IL-5 and other cytokines tested in the lungs of HySU-challenged CRTH2^{-/-} mice (such as IFN- γ , TNF- α , and IL-6; unpublished data).

CRTH2 deletion attenuates the development of PAH induced by HyOA or *Schistosoma mansoni* egg in mice

OVA can induce experimental lung diseases in animals by activating Th2 cells (Gras et al., 2013). We then tested another classical mouse PAH model induced by HyOA (Daley et al., 2008; Mizuno et al., 2012). After a nearly 5-wk exposure to chronic hypoxia (10% O₂) with OVA administration (Fig. 4 A), mice developed a prominent elevation in RVSP (Fig. 4 B) and in RV/LV + S ratio (Fig. 4 C) when compared with that observed in control mice. Again, CRTH2^{-/-} mice displayed a remarkable reduction in RVSP (31.7 ± 1.1 mm Hg vs. 42.2 ± 1.6 mm Hg, P < 0.01; Fig. 4 B) and in RV/LV + S (32.3 ± 1.1% vs. 48.3 ± 1.8%, P < 0.01; Fig. 4 C). Similarly, CRTH2 deletion ameliorated pulmonary vascular remodeling induced by HyOA (Fig. 4, D and E) through reducing pulmonary SMA-expressing cells in the medial layer (Fig. 4, F–I) but not von Willebrand factor (vWF⁺) endothelial cells in the intima (not depicted). Moreover, CRTH2 deficiency reduced PASMC proliferation in PAs in HyOA-challenged mice (Fig. 4, J and K). However, we observed no significant difference in extracellular matrix accumulation in PAs and PASMC size (unpublished data) between CRTH2^{-/-} and WT mice after HyOA challenge. Also, CRTH2 deletion had no significant influence on histological structure and contractile activity of aorta in HyOA-treated mice (unpublished data). A marked decrease in CD4⁺ T cells around PAs detected by immunostaining (Fig. 5, A and B) and in the proportions and number of Th2 cells (CD4⁺IL-4⁺ cells) in mononuclear cells from lung tissues (Fig. 5, C–E) was observed in HyOA-treated CRTH2^{-/-} mice compared with that in WT controls, whereas no significant change was observed in perivascular macrophages and neutrophils in HyOA-treated CRTH2^{-/-} mice (not depicted). Th2 cytokines in the serum (Fig. 5 F) and BALF (Fig. 5 G) were dramatically inhibited in HyOA-treated CRTH2^{-/-} mice. Among Th1, Th2, and Th17 cytokines tested, IL-4 and IL-13 expression was also suppressed in lung tissues from CRTH2^{-/-} mice after HyOA treatment (unpublished data). Moreover, CRTH2 deficiency significantly reduced the frequencies of Th2 effect cells such as mast cells and IgE-producing B cells in BALF, peripheral blood, and lung tissues in HyOA-treated mice (Fig. S1, A–F). In

addition, CRTH2 deletion suppressed expression of GATA3 of T cells in HyOA-treated mice without affecting expression of other transcription factors, such as Tbx21, GATA2, RORC, and Foxp3 (unpublished data).

Schistosoma mansoni exposure leads to prototypical Th2 inflammation, and Schistosomal infection is one of major causes of PAH worldwide (Butrous et al., 2008). We investigated the role of CRTH2 in *Schistosoma mansoni* egg-induced PAH in mice as previously described (Kumar et al., 2015). Consistently, CRTH2 deficiency conferred significant protections against *Schistosoma mansoni* egg-induced PAH in mice by suppression of Th2 immune response (unpublished data). Taken together, these results suggest that CRTH2-mediated Th2 immune response may contribute to the development of PAH in mice.

Treatment with anti-IL-4 and anti-IL-13 antibodies prevents the development of HyOA-induced PAH in WT BM-reconstituted CRTH2^{-/-} chimeric mice

To test whether CRTH2 deficiency attenuated the progression of PAH in mice through suppression of Th2 cytokine secretion, we transplanted both CRTH2^{-/-} and WT BM from enhanced GFP (EGFP) transgenic mice into irradiated CRTH2^{-/-} recipient mice and treated them with anti-IL-4 and anti-IL-13 antibodies. Genotyping of both tail biopsy specimens and blood samples from the recipient mice confirmed successful BM reconstitution (Fig. S3 A), and the efficacy of reconstitution was detected by flow cytometry (Fig. S3 B). Anti-IL-4 and/or IL-13 neutralization antibodies were infused into mice just after the second OVA challenge (Fig. S3 C). Clearly, BM replacement rectified the reduced CD4⁺ T cells in the lungs of CRTH2^{-/-} chimeric mice after HyOA challenge (Fig. S3, D and E). Consequently, the repressed protein levels of Th2 cytokines (IL-4 and IL-13) in the serum (Fig. S3, F and G) and BALF (Fig. S3, I and J) were also recovered in WT→KO group mice, whereas other cytokines remained unaltered (IFN- γ , Fig. S3, H and K; TNF- α and IL-6, not depicted). The elevated IL-4 and IL-13 levels in both the serum (Fig. S3, F and G) and BALF (Fig. S3, I and J) were effectively neutralized in HyOA models by anti-IL-4 and anti-IL-13 antibodies. Interestingly, as previously reported (Yang et al., 2005), single neutralization of IL-4 or IL-13 also reduced the other to a certain degree (Fig. S3, F, G, I, and J), which may be because of the synergistic action of IL-4 and IL-13.

Similarly, WT→KO mice developed significant increases in RVSP and RV/LV + S, compared with KO→KO mice, and these increases were notably offset by neutralization of IL-4 or IL-13, even further by their combination (Fig. S4, A and B). Pulmonary arterial remodeling was also more severe in WT→KO mice than in KO→KO mice (Fig. S4, C and D), along with increased SMA⁺ cells and PASMC proliferation in PAs (Fig. S4, E–H). Again, depletion of IL-4 or IL-13 attenuated the pathological remodeling of PAs (Fig. S4, C–F) and inhibited the increased PASMC proliferation (Fig. S4, G and H) in WT→KO mice. Moreover, treatment with IL-4 and IL-13 dual antibodies retarded the progression of HyOA-induced PAH in mice more efficiently than treatment with each single antibody (Fig. S4). Therefore, these results suggested that CRTH2-mediated secretion of IL-4 and IL-13 is implicated in the progression of PAH in mice.

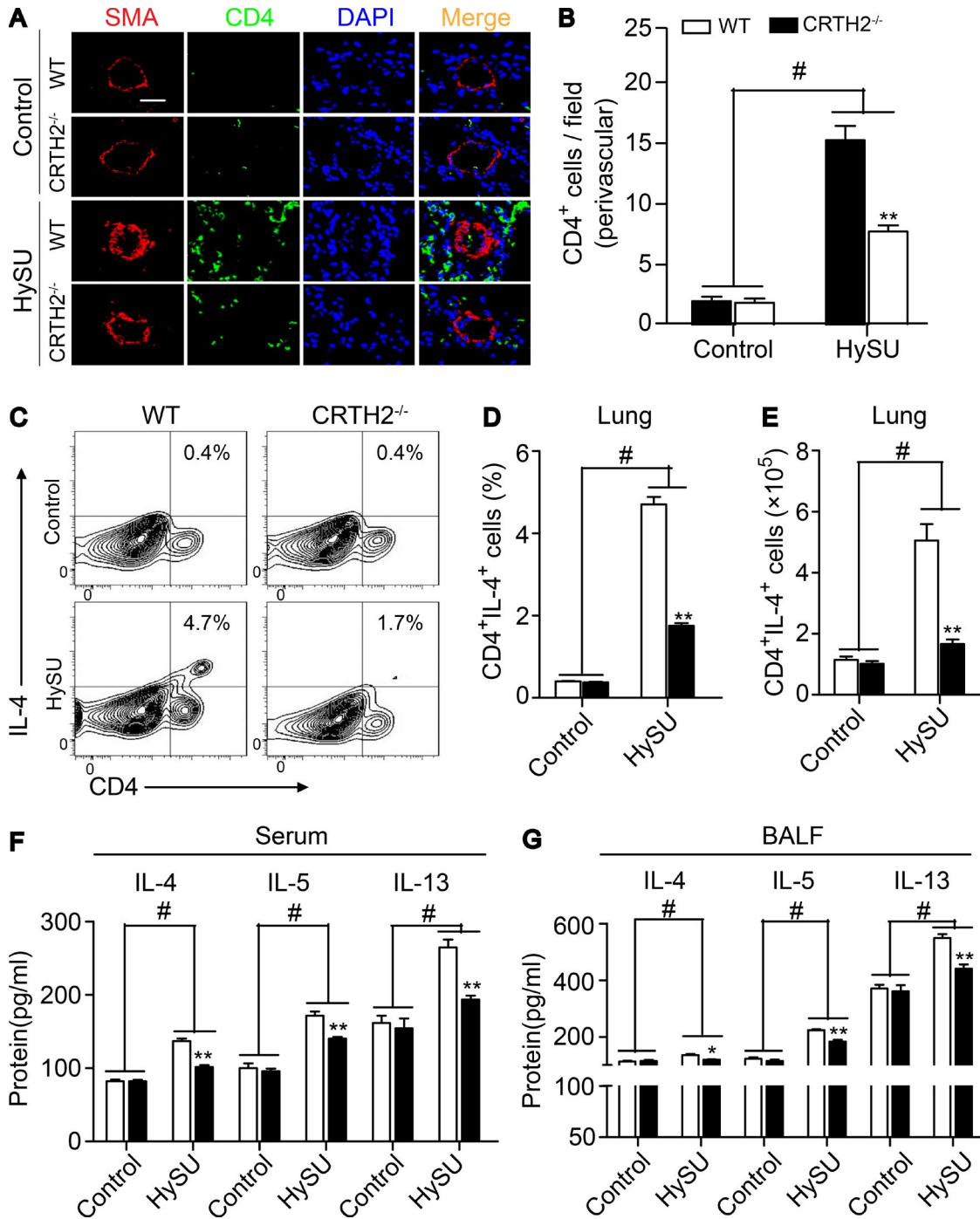


Figure 3. CRTH2 deletion suppresses Th2 immune responses in the lungs of HySU-treated mice. (A) Representative immunostaining images of CD4 (green) and SMA (red) in the lung sections from HySU-treated WT and CRTH2^{-/-} mice. Bar, 20 μm. (B) Quantification of perivascular CD4⁺ cells in the lungs as shown in A. (C–E) Representative flow cytometry charts (C) and quantification of the frequency (D) and number (E) of CD4⁺IL-4⁺ cells in lung tissues from HySU-challenged WT and CRTH2^{-/-} mice. (F and G) Quantification of IL-4, IL-5, and IL-13 levels in the peripheral blood (F) and BALF (G) by ELISA. In A–G, n = 8–10 mice per group. *, P < 0.05; **, P < 0.01 versus WT; and #, P < 0.05 versus control. Data are shown as mean ± SEM and are representative of at least two independent experiments. Statistical analysis was performed using a two-way ANOVA followed by a Bonferroni post hoc test and unpaired Student's *t* test.

Adoptive transfer of CD4⁺ T cells facilitates the progression of HyOA-induced PAH in CRTH2^{-/-} mice

CD4⁺ T cell activation was reduced in HySU- and HyOA-challenged CRTH2^{-/-} mice with much lower PA pressure compared with those in WT mice (Figs. 2, 3, 4, and 5). We next investigated whether infusion of additional purified normal CD4⁺ T cells

(Fig. 6 A) could reproduce the severe CD4⁺ T cell infiltration in the lungs and HyOA-induced PAH in CRTH2^{-/-} mice. No significant change in RVSP and RV/LV + S ratio was observed after WT CD4⁺ cell infusion in WT mice (Fig. 6, B and C), whereas WT CD4⁺ T cell transfer to CRTH2^{-/-} mice markedly augmented RVSP and RV/LV + S ratio comparable to these in vehicle-treated

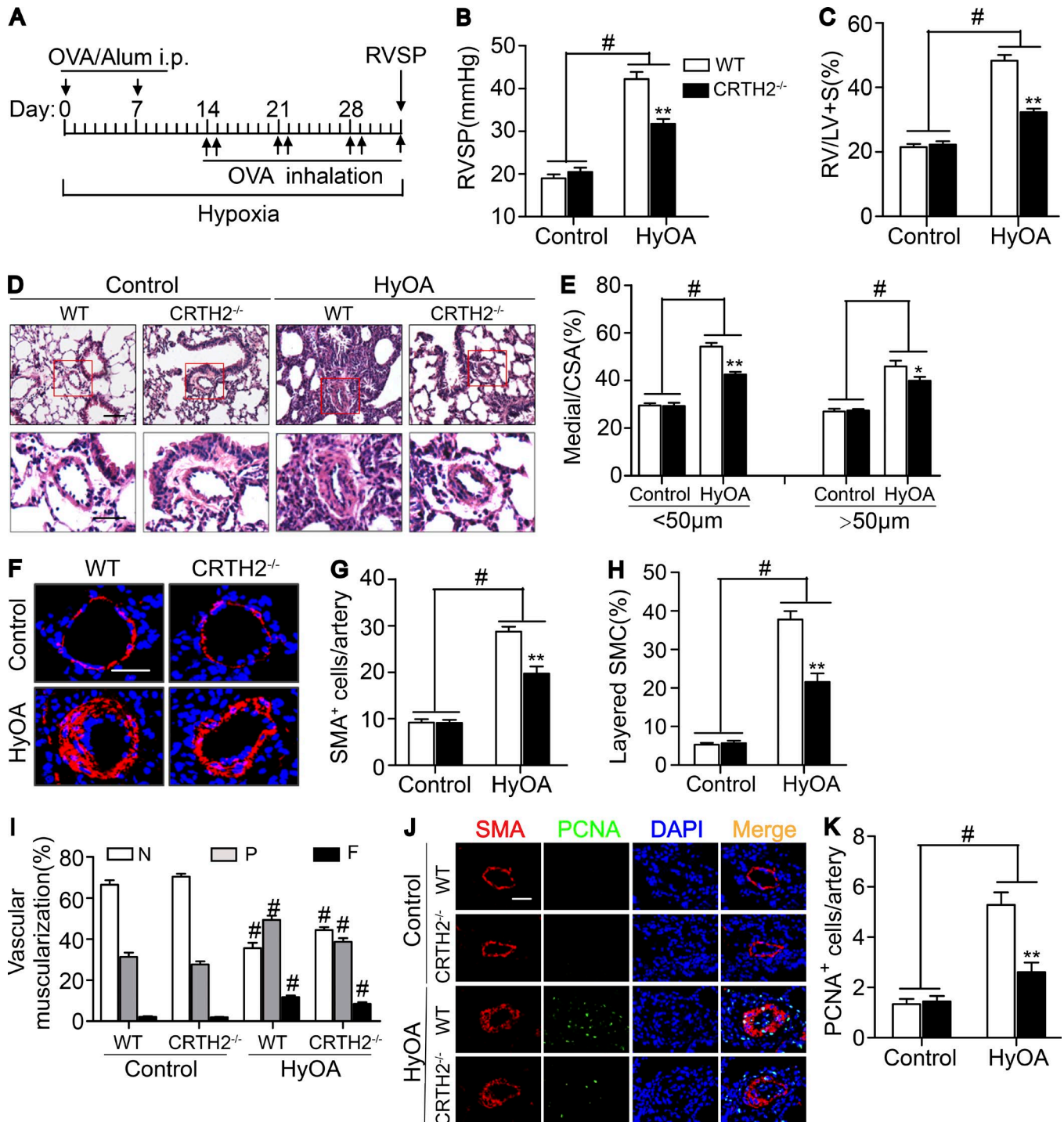


Figure 4. Disruption of CRTH2 receptor ameliorates the progression of HyOA-induced PAH in mice. (A) Protocol for HyOA-induced PAH in mice. (B and C) Effect of CRTH2 deletion on RVSP (B) and RV/LV + S ratio (C) in WT and CRTH2^{-/-} mice after HyOA treatment. (D) Representative images of H&E staining of lung sections from HyOA-treated CRTH2^{-/-} and WT mice. Bar, 20 μm. (E) Quantification of the ratio of pulmonary arterial medial thickness to total vessel size (media/CSA) for the HyOA treatment models. (F) SMA immunostaining of pulmonary vessels (20–50 μm in diameter). Bar, 20 μm. (G and H) Quantification of the number (G) and percentage (H) of layered SMCs in PAs from HyOA-treated mice. (I) Proportion of nonmuscularized (N), partially muscularized (P), or full (F) muscularized pulmonary arterioles (20–50 μm in diameter) from HyOA-treated mice. (J) Representative images of PCNA (green) and SMA (red) immunostaining of lung tissues from HyOA-treated mice. Bar, 20 μm. (K) Quantification of PCNA⁺ cells in PAs. In A–K, *n* = 8–12 mice per group. *, *P* < 0.05; **, *P* < 0.01 versus WT; and #, *P* < 0.05 versus control. All data are expressed as mean ± SEM derived from two independent experiments. *P* values were calculated using two-way ANOVA followed by a Bonferroni post hoc test or unpaired Student's *t* test.

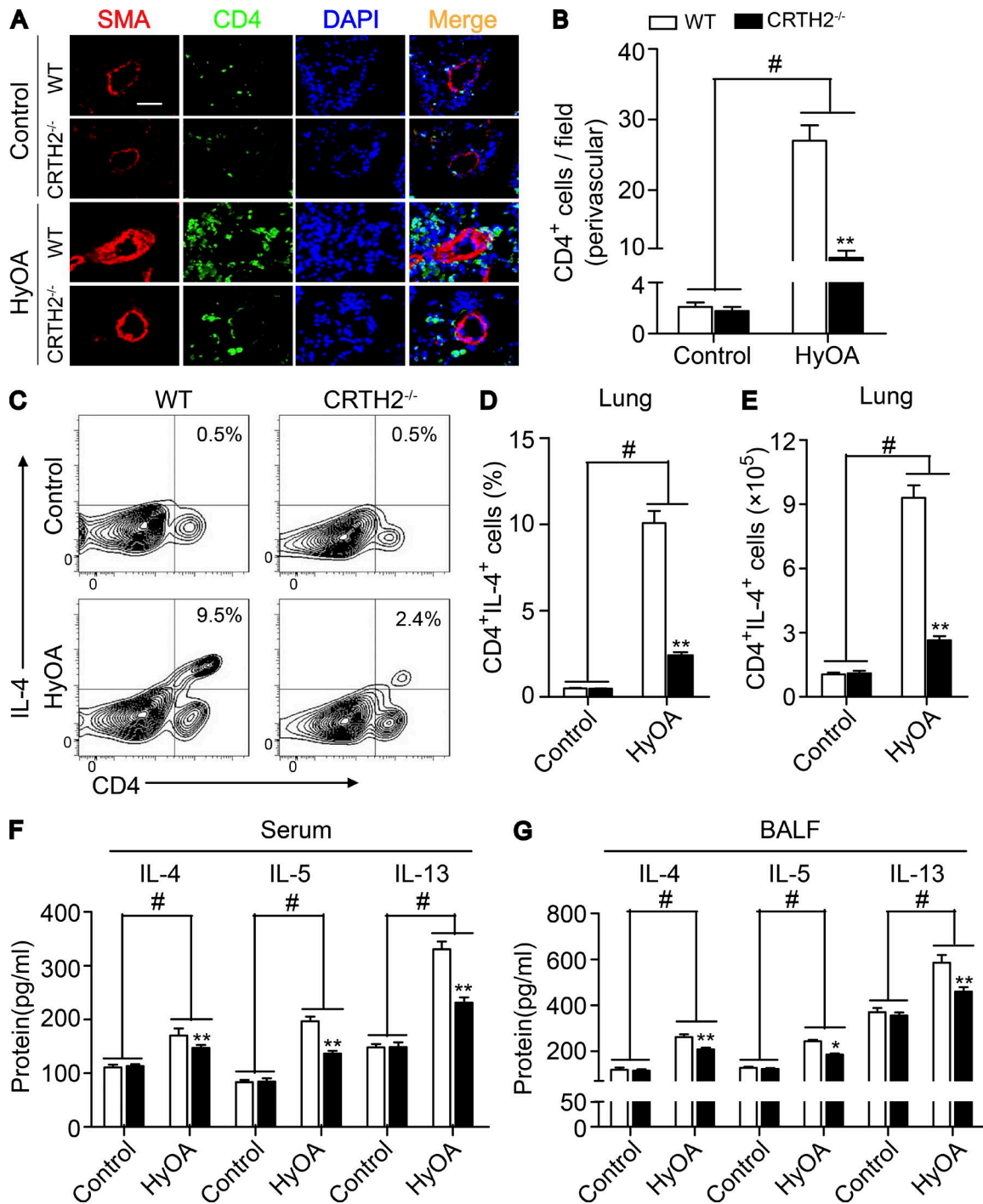


Figure 5. **CRTH2** knockout reduces Th2 immune responses in the lungs of HyOA-treated mice. (A) Representative immunostaining images of CD4 (green) and SMA (red) in lung sections from HyOA-treated WT and CRTH2^{-/-} mice. Bar, 20 μm. (B) Quantification of perivascular CD4⁺ cells in lung tissues as shown in A. (C–E) Representative flow cytometry charts (C) and quantification of the frequency (D) and number (E) of CD4⁺IL-4⁺ cells in lung tissues from HyOA-treated WT and CRTH2^{-/-} mice. (F and G) Quantification of IL-4, IL-5, and IL-13 levels in peripheral blood (F) and BALF (G) by ELISA. In A–G, n = 8–12 mice per group. *, P < 0.05; **, P < 0.01 versus WT; and #, P < 0.05 versus control. Representative data are shown as mean ± SEM derived from two independent experiments. Statistical significance was determined using two-way ANOVA followed by a Bonferroni post hoc test or unpaired Student’s *t* tests.

CRTH2^{-/-} mice after HyOA challenge (Fig. 6, B and C). Moreover, exacerbated pulmonary arterial remodeling was detected in CRTH2-deficient mice by infusion of additional WT CD4⁺ T cells, as evidenced by thickening of the medial layer of PAs with more SMA⁺ cells (Fig. 6, D–F). In addition, PASM

CG proliferation in pulmonary vessels was augmented in HyOA-treated CRTH2^{-/-} mice by infusion of extra WT CD4⁺ T cells (Fig. 6, G and H). As expected, WT CD4⁺ cell infusion in CRTH2^{-/-} mice restored the Th2 response in lung tissues after HyOA challenge. This included increased CD4⁺ cell infiltration in perivascular regions (Fig. 6,

G and I) and elevated Th2 cytokine secretion in the peripheral blood (Fig. 6J) and BALF (Fig. 6K). WT CD4⁺ cells infusion in WT mice increased IL-13 levels in serum but not in BALF (Fig. 6K). In addition, adoptive transfer of CRTH2^{-/-} CD4⁺ cells had no effect on RVSP and RV/LV + S ratio in both CRTH2^{-/-} and WT mice after HyOA challenge (Fig. 6, L-N).

Dual neutralization of IL-4 and IL-13 (Fig. 7A) effectively depleted the elevated levels of IL-4 and IL-13 in serum and BALF of CRTH2^{+/+} CD4⁺ T cell-infused CRTH2^{-/-} mice (Fig. 7, B and C) and reduced recruitment of IgE-producing B cells and mast cells in lungs in CRTH2^{+/+} CD4⁺ T cell-infused CRTH2^{-/-} mice (not depicted). Again, neutralizing anti-IL-4 and anti-IL-13 antibodies significantly attenuated the increased RVSP (Fig. 7D) and RV/LV + S ratio (Fig. 7E) and reversed pulmonary arterial wall thickness (Fig. 7, F and G) and muscularization (Fig. 7, H-J) in CRTH2^{+/+} CD4⁺ T cell-infused CRTH2^{-/-} mice. Collectively, adoptive transfer of CRTH2-expressing CD4⁺ T cells reproduced PAH pathological alterations in CRTH2^{-/-} mice as in WT mice, which was reversed by anti-IL-4/IL-13 dual neutralizing antibodies, highlighting the role of CRTH2 in the regulation of chemotactic migration and Th2 cytokine secretion of CD4⁺ T cells that contributed to pulmonary arterial remodeling and pulmonary hypertension.

Th2 cell-derived IL-4 and IL-13 promote PASMC proliferation via STAT6 activation

IL-4 and IL-13 activate many common signaling pathways such as STAT6 phosphorylation (p-STAT6) through binding their own receptors (IL-4R α , IL-13R α 1, or IL-13R α 2; Jiang et al., 2000). IL-4- and IL-13-mediated STAT6 signaling is implicated in the proliferation of vascular SMCs (Wei et al., 2000). The expression of IL-4R α , IL-13R α 1, and IL-13R α 2 is up-regulated in PAs upon HyOA treatment (Fig. 8A). p-STAT6 expression was dramatically reduced in lung tissues (Fig. 8B) and in PAs (Fig. 8C) from HyOA-treated CRTH2^{-/-} mice compared with that in WT mice. Moreover, CRTH2^{+/+} BMT restored p-STAT6 expression in PAs in CRTH2^{-/-} mice after HyOA challenge, but this up-regulation of p-STAT6 expression in PAs in CRTH2^{-/-} mice was attenuated by infusion of neutralization antibodies against IL-4 and IL-13 (Fig. 8D).

Next, we examined whether CRTH2-mediated Th2 cells directly promote PASMC proliferation through IL-4 and IL-13 using a coculture system in hypoxic atmosphere (1% O₂/5% CO₂). Purified CD4⁺ T cells were induced to differentiate to Th2 cells in culture. CRTH2 agonist 13,14-dihydro-15-keto PGD₂ (DK-PGD₂) boosted IL-4 and IL-13 secretion in Th2 cells (Fig. 8E). Interestingly, the culture medium from DK-PGD₂-stimulated Th2 cells significantly accelerated PASMC growth compared with untreated Th2 cell control medium, which was completely blocked by IL-4 and IL-13 neutralization (Fig. 8F). Proliferating cell nuclear antigen (PCNA) and SMA immunostaining also indicated that IL-4 and IL-13 antibodies abrogated the enhanced proliferation of PASMCs in DK-PGD₂-stimulated Th2 cell medium (Fig. 8, G and H). Similarly, a STAT6 inhibitor (AS1517499) also efficiently prevented the increased proliferation of PASMCs cocultured with DK-PGD₂-stimulated Th2 cells (Fig. 8, I and J).

CRTH2 inhibitor CAY10595 and neutralizing anti-IL-4 and anti-IL-13 antibodies protects against HyOA-induced PAH in mice

We then tested the effect of CRTH2 inhibitor CAY10595 on progression of HyOA-induced PAH in mice. As shown in Fig. S5, CAY10595 administration (Fig. S5A) dramatically reduced RVSP (Fig. S5B) and RV/LV + S ratio (Fig. S5C) and suppressed PA remodeling (Fig. S5, D-G) in HyOA-treated mice. Consistently, CAY10595 treatment also decreased perivascular infiltration of CD4⁺ T cells in lung tissues (Fig. S5, H and I) and Th2 cytokine secretion in both serum (Fig. S5J) and BALF (Fig. S5K) in HyOA-challenged mice. These results indicate that CRTH2 inhibitor can alleviate the progression of PA remodeling and PAH induced by HyOA by suppression of Th2 activity.

Then we assayed the effect of CRTH2 inhibitor CAY10595 and neutralizing antibodies of IL-4 and IL-13 on established PAH induced by HyOA in mice. CAY10595 administration (Fig. 9A) significantly alleviated the established PAH with declining RVSP (Fig. 9B) and RV/LV + S ratio (Fig. 9C) and reduced PA remodeling (Fig. 9, D-F). In addition, similar protective effects were observed on established PAH in mice by using neutralizing antibodies of IL-4 and IL-13. The mice treated with neutralizing anti-IL-4 and anti-IL-13 antibodies (Fig. 9G) displayed reduced RVSP (Fig. 9H) and ratio of RV/LV + S (Fig. 9I), as well as attenuated PA remodeling (Fig. 9, J-L). Taken together, CRTH2 receptor may be a promising therapeutic target for PAH.

Discussion

Increased numbers of CD4⁺ Th cells are observed in the lungs of patients with PAH (Savai et al., 2012). Here we found that Th2, not Th1, immune responses were elevated in the plasma of patients with idiopathic PAH, and the expression of the Th2 surface chemoattractant receptor, CRTH2, was also increased in CD4⁺ T cells in patients with idiopathic PAH and PAH mouse models. Genetic ablation or pharmacological inhibition of CRTH2 ameliorated experimental PAH in mice by reducing Th2 immune responses. CRTH2^{+/+} BMT and T cell adoptive transfer facilitated HyOA-induced PAH in mice through enhancing Th2 immune reaction and IL-4/IL-13 secretion. Thus, CRTH2-mediated Th2 activation contributed to the development of PAH, especially allergy-associated PAH. These observations indicate that inhibition of CRTH2 receptor may be a promising therapeutic strategy for PAH.

Perivascular inflammatory infiltrates, including macrophages, dendritic cells, and T and B cells, are often observed along with pulmonary vascular lesions in the lungs of patients with severe pulmonary hypertension (Price et al., 2012). Similar pulmonary inflammatory alterations occur in experimental PAH models such as monocrotaline-treated rats (Dorfmüller et al., 2003; Ito et al., 2007) and mice exposed to hypoxia (Frid et al., 2006). Likewise, mean perivascular inflammation score is correlated with intima plus media remodeling in the lungs of patients with idiopathic PAH (Stacher et al., 2012). Beside immune cell infiltration in the lungs, elevated serum levels of cytokines (IL-1 β , IL-6, and IL-8) and chemokines (MCP-1 and RANTES) were also reported in patients with idiopathic PAH (Rabinovitch et al., 2014). We found marked increases of circulating CD3⁺CD4⁺ T cells and proinflammatory Th2 cytokines (IL-4, IL-5, and IL-13) in patients with

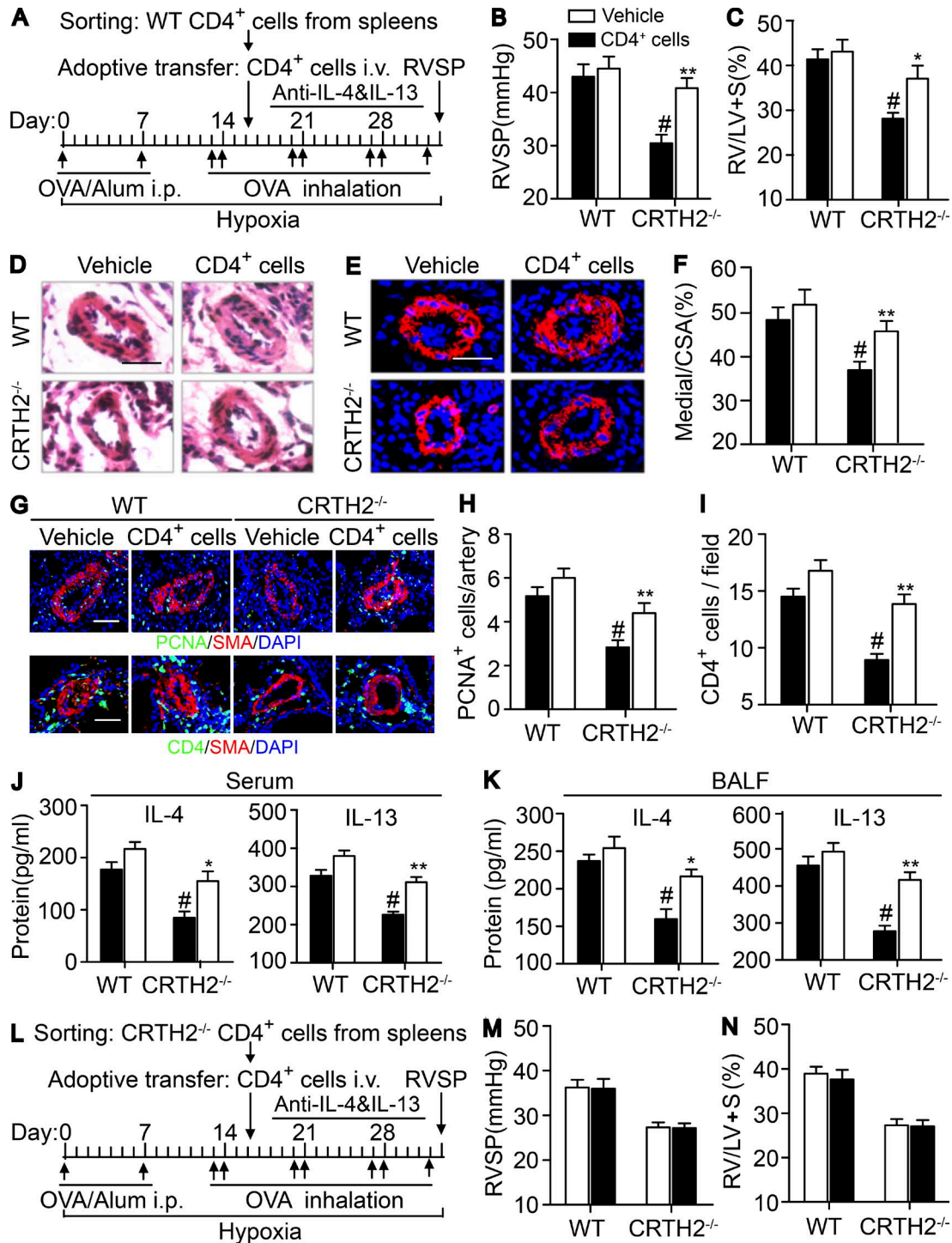


Figure 6. Adoptive transfer of CRTH2^{+/+} CD4⁺ T cells exacerbates HyOA-induced PAH in CRTH2^{-/-} mice. (A) Schematic representation of the protocol for administration of CRTH2^{+/+} CD4⁺ T cells to WT and CRTH2^{-/-} mice. (B and C) Effect of adoptive transfer of CRTH2^{+/+} CD4⁺ T cells on RVSP (B) and RV/LV + S ratio (C) of WT and CRTH2^{-/-} mice. (D and E) Representative images of H&E staining (D) and SMA (red) immunostaining (E) of lung sections of HyOA-treated CRTH2^{-/-} mice after CRTH2^{+/+} CD4⁺ T cell infusion. Bars, 20 μ m. (F) Quantification of the ratio of pulmonary arterial medial thickness to total vessel size (media/CSA). (G) Representative images of PCNA (green, top) and CD4 (green, bottom) immunostaining in lung tissues from HyOA-treated mice after CRTH2^{+/+} CD4⁺ T cell infusion. Bars, 20 μ m. (H) Quantification of PCNA⁺ cells in PAs. (I) Quantification of perivascular infiltration of CD4⁺ cells in the lungs in HyOA-treated mice after CRTH2^{+/+} CD4⁺ T cell infusion. (J and K) Quantification of secretion levels of IL-4 and IL-13 in the serum (J) and BALF (K) from HyOA-treated mice after CRTH2^{+/+} CD4⁺ T cell infusion. In A–K, $n = 8$ –10 mice per group. *, $P < 0.05$; **, $P < 0.01$ versus vehicle; and #, $P < 0.05$ versus WT. (L) The protocol for administration of CRTH2^{-/-} CD4⁺ T cells to WT and CRTH2^{-/-} mice. (M and N) Effect of adoptive transfer of CRTH2^{-/-} CD4⁺ T cells on RVSP (M) and RV/LV + S ratio (N) of WT and CRTH2^{-/-} mice; $n = 6$ –8 mice per group. Data are presented as mean \pm SEM and are representative of two independent experiments. Statistical significance was determined using two-way ANOVA followed by a Bonferroni post hoc test and unpaired Student's t tests.

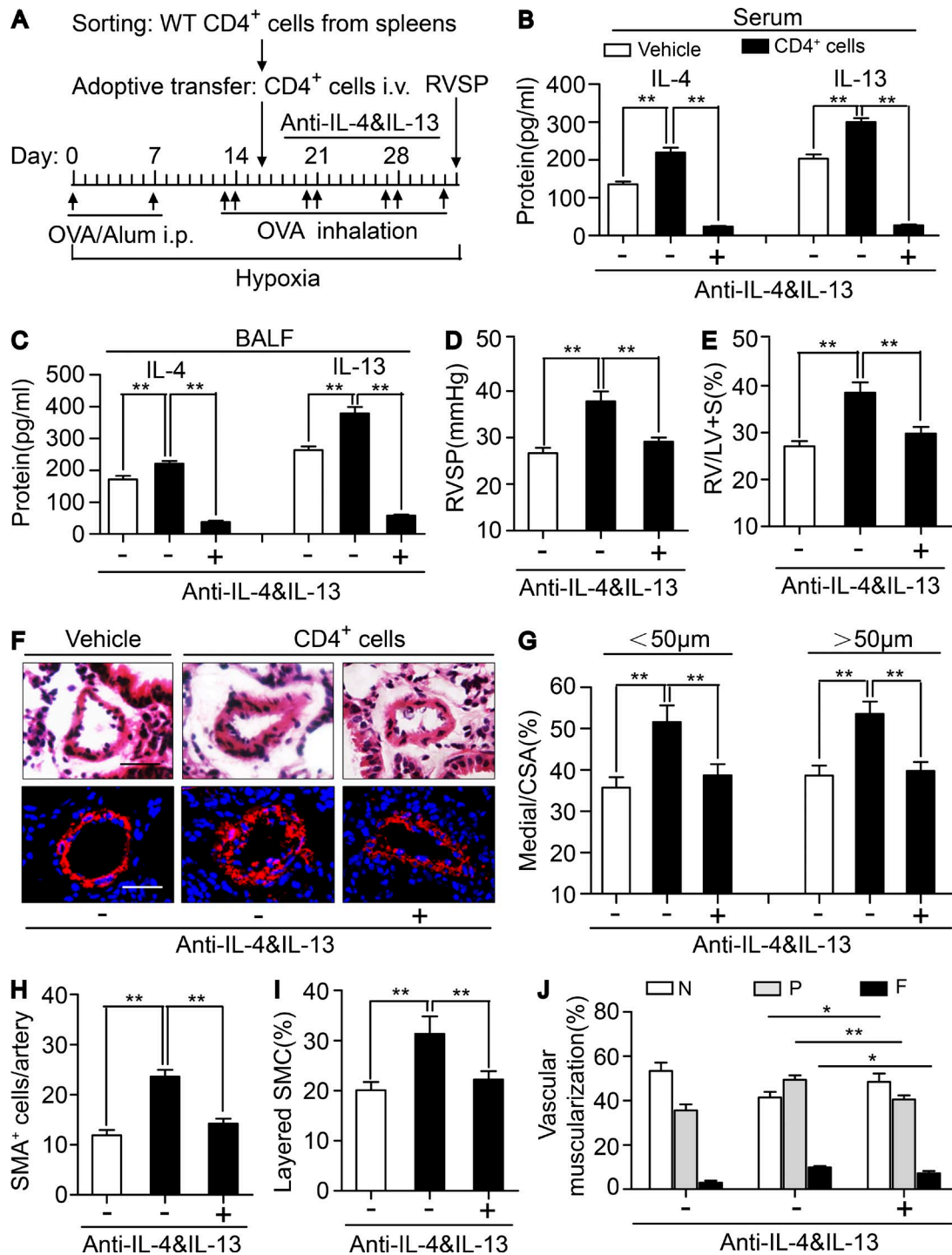


Figure 7. Neutralization of IL-4 and IL-13 reversed infusion of CRTH2^{+/+} CD4⁺ T cells exaggerated PAH in CRTH2^{-/-} mice. (A) Schematic representation of the protocol for administration of CRTH2^{+/+} CD4⁺ T cell-infused CRTH2^{-/-} mice to induce PAH. (B and C) Protein levels of IL-4 and IL-13 in the serum (B) and BALF (C) from HyOA-treated mice after CRTH2^{+/+} CD4⁺ T cell infusion with or without dual neutralization of IL-4 and IL-13. (D and E) Effect of neutralization of IL-4 and IL-13 on RVSP (D) and RV/LV + S ratio (E) in CRTH2^{+/+} CD4⁺ T cell-infused CRTH2^{-/-} mice. (F) Representative images of H&E staining and SMA (red) immunostaining of PAs of CRTH2^{+/+} CD4⁺ T cell-infused mice with or without dual neutralization of IL-4 and IL-13. Bar, 20 μm. (G) Quantification of the ratio of pulmonary arterial medial thickness to total vessel size (media/CSA) for the CRTH2^{+/+} CD4⁺ T cell-infused mice with or without dual neutralization of IL-4 and IL-13. (H and I) Quantification of the number (H) and percentages (I) of layered SMCs in PAs from CRTH2^{+/+} CD4⁺ T cell-infused mice with or without dual neutralization of IL-4 and IL-13. (J) Proportion of nonmuscularized (N), partially muscularized (P), or full muscularized (F) pulmonary arterioles (20–50 μm in diameter) from CRTH2^{+/+} CD4⁺ T cell-infused mice with or without dual neutralization of IL-4 and IL-13. In A–J, n = 8–10 mice per group. *, P < 0.05; **, P < 0.01 as indicated. All graphs are shown as mean ± SEM. Data are representative of at least two independent experiments. Statistical significance was determined using unpaired Student's *t* tests.

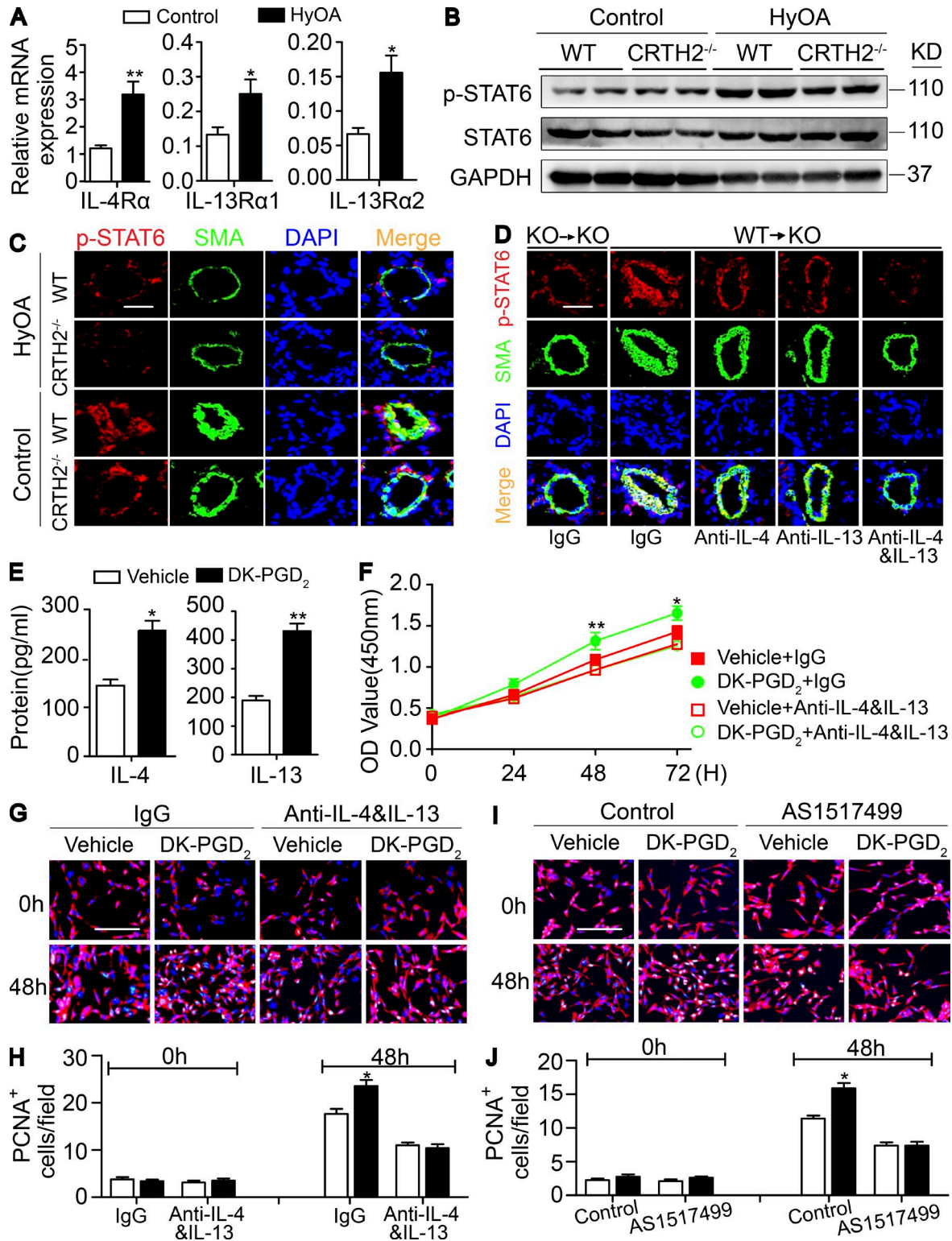


Figure 8. Th2-mediated IL-4 and IL-13 by CRTH2 activation promotes PASC proliferation through STAT6. (A) Relative mRNA expression of receptors of IL-4 and IL-13 (IL-4Ra, IL-13Ra1, and IL-13Ra2) in PAs from HyOA-treated mice. (B) Western blot analysis of phosphorylation of STAT6 (p-STAT6) in PAs isolated from HyOA-treated WT and CRTH2^{-/-} mice. (C) Representative immunostaining images of SMA (green) and p-STAT6 (red) in lung tissues from HyOA-treated PAH mouse models. Bar, 20 μm. (D) Representative immunostaining images of SMA (green) and p-STAT6 (red) in lung tissues of BM-reconstructed mice with or without dual neutralization of IL-4 and IL-13. Bar, 20 μm. In A–D, n = 6–8 mice per group. *, P < 0.05; **, P < 0.01 as indicated. (E) IL-4 and IL-13 levels in the culture medium of Th2 cells treated with CRTH2 agonist DK-PGD₂. n = 4. *, P < 0.05; **, P < 0.01 as indicated. (F) Growth curve of PASMCs cultured with DK-PGD₂-treated Th2 cell medium with or without dual neutralization of IL-4 and IL-13. n = 6. *, P < 0.05; **, P < 0.01 as indicated. (G) Representative images of PCNA (green) and SMA (red) immunostaining of PASMCs cultured with DK-PGD₂-treated Th2 cell medium with or without dual neutralization of IL-4 and

idiopathic PAH. Indeed, pulmonary hypertension also occurs in some chronic infectious diseases such as schistosomiasis and HIV (Bigna et al., 2016; Gavilanes et al., 2016) and immune disorders such as systemic sclerosis (Radstake et al., 2009), systemic lupus erythematosus (Bonelli et al., 2009), and Sjögren's syndrome (Flament et al., 2016). Therefore, inflammation and dysregulated immunity may contribute to the development of PAH, and antiinflammation therapy may represent one promising option for the treatment of severe PAH (Voelkel et al., 2016).

We and others (Harbaum et al., 2016) observed that patients with idiopathic PAH present with elevated circulating Th2 lymphocytes. Depletion of CD4⁺ T cells or Th2 immune response markedly ameliorates pulmonary arterial muscularization through suppression of Th2 cytokines, IL-4 and IL-13 (Daley et al., 2008). Interestingly, TGF- β -mediated Th2 immune response facilitates pulmonary hypertension caused by *Schistosoma mansoni* in mice (Graham et al., 2013). Double deficiency in Th2 cytokines, IL-4 and IL-13, attenuates the development of experimental *Schistosoma*-induced pulmonary hypertension in mice (Kumar et al., 2015). IL-13 signals through the heterodimer receptor complex comprised IL-4R α and IL-13R α 1, whereas IL-13R α 2 receptor acts as a competitive nonsignaling decoy receptor (Rael and Lockey, 2011). In experimental PAH models, both pharmacological inhibitor and genetic deficiency attenuate pulmonary arterial remodeling (Daley et al., 2008; Kumar et al., 2015). In contrast, lung-specific IL-13 transgenic mice spontaneously develop PAH phenotypes (Cho et al., 2013). Moreover, IL-13R α 1-deficient mice do not develop PAH, whereas IL-13R α 2-deficient mice have exacerbated pulmonary arterial remodeling and pulmonary hypertension in response to *Schistosoma mansoni* eggs (Graham et al., 2010). Consistently, IL-13R α 2 mediates inhibition of human PASMC proliferation in vitro through suppression of endothelin-1 production (Hecker et al., 2010). We and others observed that IL-13 promotes PASMC proliferation, probably through IL-13R α 1 receptor (Graham et al., 2010). CRTH2-a receptor for PGD₂, preferentially expressed in Th2 cells, mediates PGD₂-dependent chemotaxis and Th2 cell migration (Hirai et al., 2001). We found that CRTH2 ablation protects against both HySU- and HyOA-induced severe PAH in mice by suppressing Th2 infiltration and activity, and CRTH2^{+/+} BMT or CRTH2^{+/+} CD4⁺ T cell adoptive transfer promotes the development of HyOA-induced PAH in CRTH2^{-/-} mice, which is reversed by dual neutralization of IL-4 and IL-13. These observations suggest IL-4 and IL-13 may mediate the effects of CRTH2 on PAH pathogenesis. Meanwhile, Th2 cytokines also drive airway inflammatory reaction in allergic asthma (Barnes, 2018), and genome-wide association studies also link innate immune pathway and Th2 activation with pathogenesis of asthma and allergic diseases (Ober and Yao, 2011). Despite common pathological features in both asthma and PAH, such as

inflammation, smooth muscle constriction, and SMC proliferation, allergy exposure leads to remodeling of both bronchi and pulmonary vessels in rodents (Rydell-Törmänen et al., 2008a,b). BMPR2 mutations were observed in ~80% of familial and 15% of idiopathic PAH patients (Germain et al., 2013). Hypomorphic expression of BMPR2 increases sensitivity of immune response to a mild antigen and facilitates PAH development (Park et al., 2013). Vasoactive intestinal peptide deficiency results in both asthma (Szema et al., 2006) and PAH phenotypes (Said et al., 2007), again by modulating NFAT-mediated T cell function (Said et al., 2010).

Th2 activation promotes B cell through IL-4 to produce IgE antibodies, which in turn activate mast cells and eosinophils (Thiriou et al., 2017). Indeed, animal studies show eosinophils and mast cells are involved in pathogenesis of some forms of pulmonary hypertension, such as IL-33 or allergy-induced PAH (Weng et al., 2011; Ikutani et al., 2018) and flow-associated PAH (Dahal et al., 2011; Bartelds et al., 2012). CRTH2, an orphan receptor on Th2 cells, is also expressed in eosinophils (Nagata et al., 1999a), mast cells (Moon et al., 2014), and human ILC2 (Wojno et al., 2015), which may contribute to allergy-induced PAH. Indeed, CRTH2 deficiency significantly suppresses the recruitment of IgE-producing B cells and mast cells in lungs, BALF, and peripheral blood in HyOA-treated mice. Adoptive transfer of CD4⁺ T cells replicates histological and hemodynamic alterations of HyOA-induced PAH in CRTH2^{-/-} mice with augmented infiltration of IgE-producing B cells and mast cells in lungs, and neutralization of Th2 cytokines markedly alleviates established pulmonary hypertension induced by HyOA treatment in mice and significantly decreases T cell adoptive transfer-triggered infiltration of mast cells and IgE-producing B cells in lung tissues in HyOA-treated mice. These observations indicate the suppressed pulmonary recruitment of both IgE-producing B cells and mast cells is attributed to, at least partially, the reduced Th2 activity in CRTH2^{-/-} mice. However, lineage-specific excision using Cre recombinase may be required to directly dissect CRTH2 role in Th2 cells from other inflammatory cells in pathogenesis of PAH in mice.

In summary, we found that CRTH2 receptor is up-regulated in circulating CD4⁺ T cells in patients with idiopathic PAH and CRTH2-mediated Th2 activation facilitates PAH pathogenesis in experimental PAH mouse models. Therefore, CRTH2 chemokine receptor may serve as a promising therapeutic target for severe PAH.

Materials and methods

Animals

8–10-wk-old male mice were used in all experiments in this study. Both WT (CRTH2^{+/+}) and CRTH2 KO (CRTH2^{-/-}) mice were

IL-13. Bar, 200 μ m. (H) Quantification of PCNA⁺SMA⁺ PSMCs as shown in G for five to six independent experiments. (I) Representative images of PCNA (green) and SMA (red) immunostaining of PSMCs cultured with DK-PGD₂-treated Th2 cell medium with or without STAT6 inhibitor AS1517499. Bar, 200 μ m. (J) Quantification of PCNA⁺SMA⁺ PSMCs in I for five to six independent experiments. *, P < 0.05; **, P < 0.01 as indicated. All graphs are shown as mean \pm SEM. Data are representative of at least two independent experiments. Statistical significance was determined using two-way ANOVA followed by a Bonferroni post hoc test and unpaired Student's *t* tests.

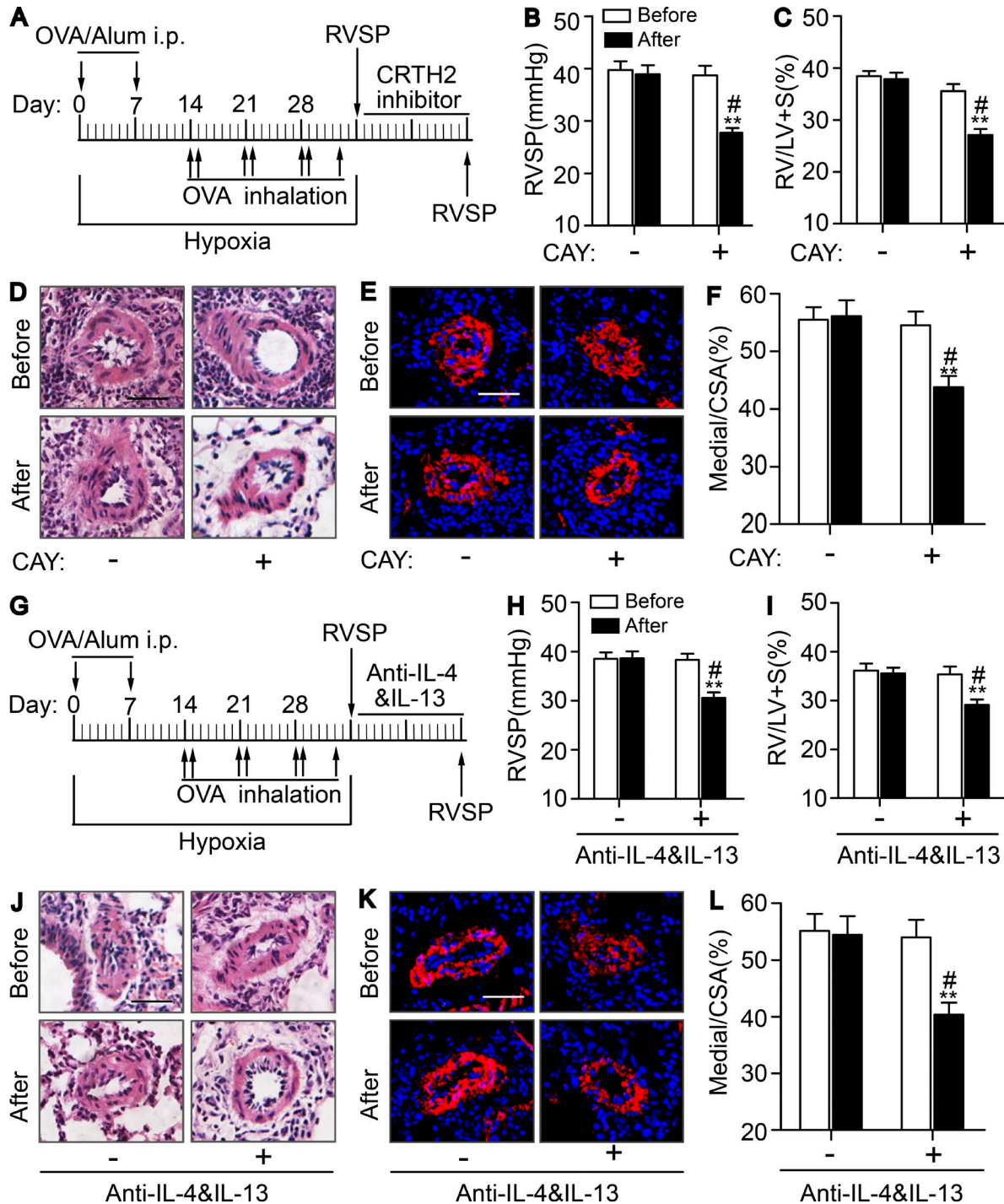


Figure 9. Pharmacological inhibition of CRTH2 receptor or dual neutralization of IL-4 and IL-13 attenuates established PAH in mice. (A) Protocol for administration of CRTH2 inhibitor CAY10595 to mice after induced by HyOA. (B and C) Effect of CAY10595 administration on RVSP (B) and RV/LV + S ratio (C) of PAH-established mice. Before, before CAY10595 treatment; After, after CAY10595 treatment; CAY, CAY10595. (D and E) Representative images of H&E staining (D) and SMA (red) immunostaining (E) of lung sections of PAH-established mice treated with CAY10595 or equivalent volume of vehicle. Bars, 20 μ m. (F) Quantification of the ratio of pulmonary arterial medial thickness to total vessel size (media/CSA) in PAs from PAH-established mice after CAY10595 treatment. In A–F, $n = 8$ –10 mice per group. *, $P < 0.05$; **, $P < 0.01$ versus vehicle (dash); #, $P < 0.05$ versus before CAY10595 treatment (Before). (G) Protocol for administration of neutralization antibodies of IL-4 and IL-13 to mice after being induced by HyOA. Before, before neutralizing treatment; After, after neutralizing treatment. (H and I) Effect of neutralization of IL-4 and IL-13 on RVSP (H) and RV/LV + S ratio (I) of PAH-established mice. (J and K) Representative images of H&E staining (J) and SMA (red) immunostaining (K) of lung sections of PAH-established mice treated with neutralization antibodies of IL-4 and IL-13 or equivalent volume of vehicle. Bars, 20 μ m. (L) Quantification of the ratio of pulmonary arterial medial thickness to total vessel size (media/CSA) in PAs from PAH-established mice after neutralization of IL-4 and IL-13. In G–L, $n = 8$ –10 mice per group. *, $P < 0.05$; **, $P < 0.01$ versus vehicle (dash); #, $P < 0.05$ versus before neutralizing treatment (Before). All graphs are shown as mean \pm SEM. Data are representative of at least two independent experiments. Statistical significance was determined using two-way ANOVA followed by a Bonferroni post hoc test and unpaired Student's t tests.

maintained on a C57BL/6 genetic background. WT littermates were generated as experimental controls from CRTH2 receptor heterozygous matings. All the mice were housed in specific pathogen-free conditions at the animal facility of the Institute for Nutritional Sciences, Chinese Academy of Sciences. All animal experiments were performed according to Guidelines of the Institutional Animal Care and Use Committee of the Institute for Nutritional Sciences, Chinese Academy of Sciences.

Reagents

SU5416 (a VEGFR2 inhibitor) and OVA were purchased from Sigma-Aldrich. DK-PGD₂ and CAY10595 (CRTH2 inhibitor) were obtained from Cayman Chemical. Anti-IL-4 and anti-IL-13 antibodies were purchased from R&D Systems. AS1517499 (a STAT6 inhibitor) was purchased from MedChemExpress.

Study population

Patients with PAH were recruited from outpatients in the Department of Pulmonary Medicine of Shanghai Ruijin Hospital from August 2014 to May 2017 (Table 1). All patients were given diagnoses based on the criteria for PAH according to the European Society of Cardiology/European Respiratory Society (ESC/ERS) guidelines for the diagnosis and treatment of pulmonary hypertension. All patients with PAH were diagnosed for the first time without any drug therapies. Subjects with tumor, autoimmune diseases, renal/liver dysfunction, or respiratory tract infection within 4 wk were excluded from the study. Age-matched healthy volunteers were recruited from the social crowd. This study was supported by the Ethics Committee of the Institute for Nutritional Sciences, Shanghai Institutes for Biological Sciences, Chinese Academy of Sciences, and the Ethics Committee of Ruijin Hospital, Shanghai Jiao Tong University School of Medicine. All participants provided written informed consent.

Chronic HySU-induced PAH in mice

8–10-wk-old WT and CRTH2^{-/-} male mice received a single weekly subcutaneous injection of SU5416 that was suspended in carboxymethylcellulose solution (0.5% [wt/vol] carboxymethylcellulose sodium, 0.9% [wt/vol] sodium chloride, 0.4% [vol/vol] polysorbate80, and 0.9% [vol/vol] benzyl alcohol in deionized water), as previously reported (Ciuclan et al., 2011). Experimental animals were exposed to chronic hypoxia (10% O₂) in a ventilated chamber for 3 wk (Wang et al., 2013). Control mice received vehicle instead of SU5416 and remained in a normoxic environment. At the end of the treatment, mice were anesthetized, hemodynamic changes were detected, and samples were collected.

Chronic HyOA-induced PAH model in mice

8-wk-old WT and CRTH2^{-/-} male mice received a single intraperitoneal injection of OVA (Sigma-Aldrich) that was diluted to 1 mg/ml in 0.15 M sterile saline (Sigma-Aldrich) and complexed with Alum (Imject Alum; Thermo Fisher Scientific; final dose, 50 μg OVA and 2 mg Alum) on the first day of the first 2 wk of treatment, as shown in Fig. 4 A. Then, the animals were challenged with aerosolized OVA for 30 min at a concentration of 10 mg/ml twice per week on the first and last day of each week during the treatment period (Daley et al., 2008; Mizuno et al.,

2012). Experimental animals were exposed to chronic hypoxia (10% O₂) in a ventilated chamber for ~5 wk. Control mice received vehicle and remained in a normoxic environment. At the end of the treatment period, hemodynamic indexes were detected, and samples were collected.

BMT

Allogeneic BMT was conducted as previously described (Zhao et al., 2011; Shi et al., 2014; Yang et al., 2014). In short, donor WT and CRTH2^{-/-} mice with EGFP were euthanized, and BM cells were collected from femurs and tibias by flushing. After a total of 9.5 Gy of total body irradiation administered in three bursts (one 3.5-Gy dose and two 3-Gy doses administered 1.5 h apart) from a ¹³⁷Cs source (MDS Nordion), recipient mice were injected with 5 × 10⁶ BM cells from donor mice in 200 μl of sterilized PBS through the tail vein to reconstitute the hematopoietic system.

Adoptive transfer of CD4⁺ cells

WT or CRTH2^{-/-} CD4⁺ cells from mouse spleens were purified by means of magnetic cell sorting. For adoptive transfer, conducted as reported (Shi et al., 2014), 4 × 10⁶ isolated cells were injected through the tail vein to WT or CRTH2^{-/-} mice 2 d before OVA challenge.

CAY10595 treatment

CRTH2 antagonist CAY10595 (Cayman Chemical) was dissolved in Tween80/ethanol/tap water (5:5:90 vol/vol/vol). HyOA-challenged male mice (8 wk old) were given CAY10595 (5 mg/kg body weight) daily by oral gavage at days 18–30 as shown in Fig. S5 A, or after the rodent PAH model established as shown in Fig. 9 A. Control group mice were treated with the same volume of vehicle.

Analysis of RVSP and right heart hypertrophy (RV/LV + S)

Before the measurements, the mice were color coded to obscure the genotype. After mice were anesthetized, a left parasternal incision was made; then the ribs were partially resected, a 1.4-F microtip pressure transducer catheter (Millar Instruments) was carefully inserted into the RV, and RVSP was continuously monitored for 5 min using a PowerLab data acquisition system (AD Instruments). RV hypertrophy was assessed by Fulton index measurements (weight of RV/LV + S).

IL-4 and IL-13 immunoneutralization

The BM-reconstituted mice or CD4 T cell-transferred mice were intraperitoneally injected with neutralizing antibodies against IL-4 (0.5 mg per mouse; Mabalirajan et al., 2008) and IL-13 (0.5–1 mg per mouse; Daley et al., 2008) or control IgG protein just after the second OVA challenge per week as shown in Fig. S3 C and Fig. 7 A or after the PAH established with the same timing as shown in Fig. 9 G.

RNA extraction and real-time PCR

Total RNA from isolated CD4⁺ T cells from peripheral blood of patients with PAH and lung tissues from mouse PAH models was extracted by RNeasy Mini kit (Qiagen). Total RNA from lung homogenates was extracted by using TRIzol reagent (Invitrogen), according to the manufacturer's protocols. In brief, total

RNA (1 µg) was reverse-transcribed to cDNA by using Reverse Transcription Reagent kits (Takara Bio Inc.), according to the manufacturer's instructions. The resulting cDNA was amplified with 40 cycles by real-time PCR. Each sample was analyzed in triplicate and normalized to a reference RNA within the sample. Sequences of primers for real-time PCR analysis for human samples were as follows: Fw-IL-4: 5'-TCTTTGCTGCCTCCAAGA ACAC-3', Re-IL-4: 5'-GGTTCCTGTGAGCCGTTTC-3'; Fw-IL-13: 5'-CCTGATCAACGTGTCAGGCT-3', Re-IL-13: 5'-TGAAGTGTCCCT CGCGAAAA-3'; Fw-TNF-α: 5'-TCTTCTCGAACCCCGAGTGA-3', Re-TNF-α: 5'-ATGAGGTACAGGCCCTCTGA-3'; Fw-DPI: 5'-ATG CGCAACCTCTATGCGAT-3', Re-DPI: 5'-GCGCGATAAATTACGGGAG-3'; Fw-EPI: 5'-CACCTTCTTTGGCGGCTCTC-3', Re-EPI: 5'-CTC CAGCAGATGCACGACA-3'; Fw-TP: 5'-GGTCTTCATCGCCAGAC AG-3', Re-TP: 5'-CACGCGCAAGTAGATGAGCA-3'; Fw-β-actin: 5'-GAGAAAATCTGGCACCACACC-3', Re-β-actin: 5'-GGATAGCAC AGCCTGGATAGCAA-3'. Fw-IL-5: 5'-TCTACTCATCGAACTCTG CTGA-3', Re-IL-5: 5'-CCCTTGACAGTTTACTCTC-3'; Fw-IL-1β: 5'-AGCTACGAATCTCGACCAC-3', Re-IL-1β: 5'-CGTTATCCCATG TGTCGAAGAA-3'; Fw-IFN-γ: 5'-TCGGTAACTGACTTGAATGTC CA-3', Re-IFN-γ: 5'-TCGCTTCCCTGTTTACTGCTGC-3'; Fw-IP: 5'-GTCAGGTCTGCTCTGGTCTG-3', Re-IP: 5'-GCTCTTGGAGTGGCT TGTA-3'; Fw-CRTH2: 5'-CCTCTGTGCCAGAGCCACGATG-3', Re-CRTH2: 5'-CACGGCCAAGAAGTAGTGAAGAAG-3'; Fw-EP2: 5'-CGATGCTCATGCTCTTCGC-3', Re-EP2: 5'-GGGAGACTGCAT AGATGACAGG-3'; Fw-EP3: 5'-CGCCTCAACCACTCCTACAC-3', Re-EP3: 5'-GACACCGATCCGCAATCCTC-3'; Fw-EP4: 5'-CCGGCG GTGATGTTTCACTT-3', Re-EP4: 5'-CCCACATACCAGCGTGTAGAA-3'; Fw-FP: 5'-AAGTCCAAGGCATCGTTTCTG-3', Re-FP: 5'-TGAATC CAATACACCGCTCAAT-3'; Fw-Tbx21: 5'-TGACTGCCTACCAGAATG CC-3', Re-Tbx21: 5'-ATTGACAGTTGGGTCCAGGC-3'; Fw-GATA2: 5'-CGCTGTGTCGGAACCAT-3', Re-GATA2: 5'-TCCATGTAG TTGTGCGCCAG-3'; Fw-GATA3: 5'-AGTTGCCGTTGAGGGTTT CA-3', Re-GATA3: 5'-TCCGAGCACAACCACCTTAG-3'; Fw-RORC: 5'-CCACAGAGACAGCACCGAG-3', Re-RORC: 5'-AGACGACTT GTCCCCACAGA-3'; Fw-Foxp3: 5'-CCTCCAGGACAGGCCACA TT-3', Re-Foxp3: 5'-ATTTGCCAGCAGTGGGTAGG-3'. Sequences of primers for real-time PCR analysis for mouse samples were as follows: Fw-IL-4: 5'-CTCGAATGTACCAGGAGCCA-3', Re-IL-4: 5'-TCGTTGCTGTGAGGACGTTT-3'; Fw-lipocalin-type PG D synthase (L-PGDS): 5'-TGGTTCGGGAGAAGAAAGC-3', Re-L-PGDS: 5'-TGGTGCCTCTGCTGAATAGC-3'; Fw-CRTH2: 5'-CAATCTCCC GGAGCAAGGTG-3', Re-CRTH2: 5'-CCAGGTAACCTCCTCGATG GC-3'; Fw-IL-4Rα: 5'-ATGCATCCCCGAGGAACAGTG-3', Re-IL-4Rα: 5'-AGCCATTGCTCGGACACATT-3'; Fw-TNFα: 5'-AAACCA CCAAGTGGAGGAGC-3', Re-TNFα: 5'-ACAAGGTACAACCCATCG GC-3'; Fw-β-actin: 5'-GTACCACCATGTACCCAGGC-3', Re-β-actin: 5'-AACGCAGCTCAGTAACAGTCC-3'; Fw-IL-5: 5'-AGCAAT GAGACGATGAGGCT-3', Re-IL-5: 5'-GTACCCACGAGGACAGTT TG-3'; Fw-IL-6: 5'-TAGTCCTTCTACCCCAATTTCC-3', Re-IL-6: 5'-TTGGTCTCTTAGCCACTCCTTC-3'; Fw-IL-13: 5'-CCTGGCTCT TGCTTGCTTGG-3', Re-IL-13: 5'-TCTTGTGTGATGTTGCTCA-3'; Fw-IFN-γ: 5'-ATGAACGCTACACACTGCATC-3', Re-IFN-γ: 5'-CCA TCCTTTTGCCAGTTCCTC-3'; Fw-H-PGDS: 5'-GGAAGAGCCGAA ATTATTCGCT-3', Re-H-PGDS: 5'-ACCACCTGCATCAGCTTGACAT-3'; Fw-DPI: 5'-GCTTTCTGTGCGCTCCCTTTG-3', Re-DPI: 5'-CAT CCGGAATACTGAAGTCCCTG-3'; Fw-IL-13Rα1: 5'-AGCGTCTCTGTC

GAAAATCTCT-3', Re-IL-13Rα1: 5'-GAGTGCAATTTGGACTGG CTC-3'; Fw-IL-13Rα2: 5'-TGGCAGTATTTGGTCTGCTCT-3', Re-IL-13Rα2: 5'-CAAGCCCTCATAACCAGAAAAACA-3'.

Western blotting

The protein concentrations of lung homogenates were determined by using a Pierce BCA Protein Assay Kit (Pierce). Equal quantities of proteins were denatured and resolved by 10% SDS-PAGE, transferred to nitrocellulose membranes, incubated with 5% skimmed milk for 1–1.5 h, and then incubated with primary antibodies overnight at 4°C. Primary antibodies were diluted as follows: phospho-STAT6 (pY641; 1:500; Santa Cruz Biotechnology), STAT6 (1:1,000; Abclonal), HIF-1α (1:1,000; Cell Signaling Technology), and GAPDH (1:2,000; Cell Signaling Technology), used as the load control. The membranes were then incubated in HRP-labeled secondary antibody in blocking buffer for 2 h at room temperature. Blots were developed by using an enhanced chemiluminescence reagent (Thermo Fisher Scientific).

Histological analysis

When hemodynamic measurements were over, the pulmonary circulatory system was flushed with chilled PBS, and the heart, aorta, and lung tissues were collected. The RV was carefully dissected from the heart and weighed. RV hypertrophy was evaluated by normalizing the weight of the RV to the weight of the LV plus septum (RV/LV + S). The left lungs were placed in liquid nitrogen for preparation of homogenates, and the lower lobes of the right lungs and aortas were fixed with 4% paraformaldehyde for 24 h. The slides (5 µm thickness) were stained with H&E for morphological analysis after paraffin embedding and sectioning. Pulmonary vascular remodeling was quantified by accessing the medial wall thickness and the percentage of muscularization. To assess the medial wall thickness, 20–25 muscular arteries, categorized as being 20–50 µm and 50–100 µm in diameter, from each lung were randomly outlined by an observer blinded to mouse genotype or pharmacological treatment. The degree of medial wall thickness, presented as a ratio of medial area to cross-sectional area (media/CSA; Lu et al., 2015), was analyzed by using ImageJ (National Institutes of Health) or Image-pro plus (Media Cybernetics). To evaluate the degree of muscularization, 30–50 intraacinar vessels at a size between 20 and 50 µm in each mouse were categorized as nonmuscular, partially muscular, or fully muscular, as previously reported (Ciucan et al., 2011). The degree of muscularization was expressed as the proportion of nonmuscular, partially muscular, or fully muscular arteries to total pulmonary vessels. Masson's trichrome staining was performed according to the manufacturer's instructions (Sigma-Aldrich).

Aortic ring assay

Mice aortas were separated and transferred immediately to Krebs' buffer (containing 4.7 mmol/L KCl, 118 mmol/L NaCl, 2.5 mmol/L CaCl₂, 1.2 mmol/L KH₂PO₄, 1.2 mmol/L MgSO₄, 11 mmol/L glucose, and 25 mmol/L NaHCO₃), cleared of fat and connective tissues while keeping the endothelium intact, cut into 2–3-mm rings, fixed on isometric force transducers (model 610 M; Danish Myo Technology) in a 5-ml organ bath, and gassed with 95% O₂

and 5% CO₂ under an initial resting tension of 3 mN. Data were recorded using the PowerLab/8sp data acquisition system (AD Instruments). After 60 min of incubation in oxygenated Krebs solution at pH 7.4 and 37°C, rings contractility was tested three times in high-K⁺ mediums (60 mM KCl) to stabilize the contraction. Cumulative concentration–response curves of acetylcholine (10⁻⁹–10⁻⁵ mol/L) were constructed with a phenylephrine pre-contraction (1 μmol/L).

Immunofluorescence staining

For immunofluorescence staining, the frozen sections (7 μm) or deparaffinized and dehydrated sections (5 μm) from tissues or glass coverslips with cells were fixed in cold acetone and washed with PBS (0.15 M, pH 7.4). The samples were treated with PBS containing 0.25% Triton X-100 for 10 min for permeabilization and then incubated with 3% BSA/PBS for 0.5–1 h to block non-specific binding of the antibodies. Next, the slides were incubated with primary antibodies specific to mouse α-SMA (diluted 1:500; Sigma-Aldrich), CD4 (diluted 1:50; eBioscience), CD68 (diluted 1:200; AbD Serotec), Mac-3 (diluted 1:100; eBioscience), Ly6G (diluted 1:100; eBioscience), EGFP (diluted 1:1,000; Abcam), PCNA (diluted 1:1,000; Cell Signaling Technology), and pY641-STAT6 (diluted 1:100; Santa Cruz Biotechnology) overnight at 4°C. Slides were then washed with PBS three times and incubated with secondary antibodies conjugated with Alexa Fluor 488, Alexa Fluor 594, or Alexa Fluor 633 (Invitrogen) for 1–2 h at room temperature. Prolong Gold antifade reagent with DAPI (Invitrogen) was used to mount and counterstain the slides. All of the fluorescence images were captured under a laser-scanning confocal microscope (Olympus) at 200× and 400×. All images were analyzed with ImageJ (National Institutes of Health) or Image-Pro Plus software (Media Cybernetics).

ELISA

Cytokine levels in serum, BALF supernatants, and cell culture medium were assayed by using ELISA, according to the manufacturer's instructions (R&D Systems).

PG extraction and analysis

Lung tissues were homogenized and centrifuged, and the supernatant (500 μl) was collected for PG extraction after protein quantification. An internal standard (2 μl) was added into each sample with 40 μl citric acid (1 M) and 5 μl of 10% butylated hydroxytoluene. Subsequently, the sample was vigorously shaken with 1 ml solvent (normal hexane: ethylacetate, 1:1) for 1 min. After centrifugation (6,000 g) for 10 min, the supernatant organic phase was collected and dried by a gentle stream of nitrogen, dissolved in 100 μl of 10% acetonitrile in water, and passed through small centrifugal filters with a 0.2-μm nylon membrane before analysis by liquid chromatography–tandem mass spectrometry. Finally, PG production was normalized to total protein.

Flow cytometric analysis

Human PBMCs and mouse white blood cells from blood, BALF, and lung tissues were analyzed by using a BD flow cytometer (FACScan; BD Biosciences). Total viable leukocyte number was determined with the trypan blue exclusion method (>90%). In

brief, the cells were harvested and incubated for ~30 min on ice with 1% BSA in PBS containing primary antibodies. For human samples, primary antibodies were diluted as follows: FITC-CD3 (1:100; Miltenyi Biotec), PE-CD4 (1:100; Miltenyi Biotec), FITC-CD4 (1:500; eBioscience), PE/Cy7-CD4 (1:200; eBioscience), APC-CD8 (1:100; Miltenyi Biotec), APC/Cy7-CCR3 (1:200; Biolegend), FITC-CD123 (1:200; Biolegend), Brilliant Violet 421-CD49d (1:200; Biolegend), APC-HLA-DR (1:200; Biolegend), APC-c-kit (1:200; Biolegend), PE-FcεRIα (1:200; eBioscience), eFluor 450-CD127 (1:200; Biolegend), PE/Cy7-CRTH2 (1:200), Brilliant Violet 421-CRTH2 (1:200; Biolegend), FITC-CD19 (1:200; Biolegend), eFluor 450-B220 (1:200; eBioscience), PE/Cy7-IgE (1:200; Biolegend), APC-CD25 (1:200; Biolegend), and PE-Foxp3 (1:200; eBioscience). For mouse samples, primary antibodies were diluted as follows: eFluor 450-CD3 (1:500; eBioscience), FITC-CD4 (1:500; eBioscience), PE/Cy7-CD4 (1:200; eBioscience), PE-CD8 (1:500; eBioscience) and PE/Cy7-IL-4 (1:200; eBioscience), PE/Cy7-Siglec-F (1:200; eBioscience), FITC-CCR3 (1:200; Biolegend), PE-CD123 (1:200; Biolegend), PE-c-kit (1:200; Biolegend), Alexa Fluor 647-FcεRIα (1:200; Biolegend), APC-CD19 (1:500; eBioscience), PE-IgE (1:200; Biolegend), APC-CD25 (1:200; eBioscience), and eFluor 450-FoxP3 (1:200; eBioscience). The cells were then washed twice before analysis. FCS files were exported and analyzed using FlowJo8.3.3 software (Tree Star Inc.).

Cell culture

6-wk-old mice were euthanized by CO₂ overexposure. Proximal PAs were aseptically isolated from the lung lobe and placed in DMEM (Gibco) at room temperature. After removing adhering fat, connective tissues, and endothelial cells, the dissected media of the PAs was then cut into small pieces (1–2 mm²) and covered by autoclaved glass coverslips in cell culture dishes. Primary mouse PSMCs were cultured in DMEM/F-12 (Gibco) supplemented with 20% FBS, 2 mM L-glutamine, 100 U/ml penicillin, and 0.1 mg/ml streptomycin at 37°C and 5% CO₂. The PSMCs were identified by positive immunostaining with antibodies against α-SMA (Sigma-Aldrich). Cells at passages 3–6 were used in experiments, and each experiment was repeated at least three times with different preparations. For hypoxic exposure, PSMCs were seeded in culture dishes placed in a hermetic tank with 1% O₂/5% CO₂ (Weisel et al., 2014).

Purified CD4⁺ T cells were isolated from the spleens of 6–8-wk-old mice by magnetic-activated cell sorting kit (STEMCELL Technologies). CD4⁺ T cells were differentiated into Th2 cells *in vitro* as previously described (Li et al., 2011). PSMCs were cocultured with Th2 cells by adding medium of Th2 cells to culture dishes. The proliferation of PSMCs was detected by a cell-counting kit (CCK-8; Dojindo Laboratories), according to the manufacturer's instructions.

Statistical analysis

Data analysis was performed using GraphPad Prism version 5.0. All data are expressed as the mean ± SEM. Two-tailed unpaired Student's *t* test and one- or two-way ANOVA with Bonferroni post hoc analyses were used for comparisons between different groups. *P* < 0.05 was considered statistically significant. All experiments and sample sizes were designed with adequate

power according to the literature (Bonnet et al., 2017) and our previous studies. Randomization and blind analyses were used whenever possible.

Online supplemental material

Fig. S1 shows the effect of CRTH2 deficiency on Th2 response-associated cell response in lung tissue, BALF, and peripheral blood in HyOA-induced mice. Fig. S2 displays pathological alterations of HySU-induced PAH in CRTH2^{-/-} and WT mice. Figs. S3 and S4 show effects of CRTH2^{+/-} BMT on Th2 immune response and pulmonary hypertension in HyOA-treated CRTH2^{-/-} mice. Fig. S5 shows the therapeutic effect of CRTH2 inhibitor on HyOA-induced PAH in mice.

Acknowledgments

We thank Dr. Masataka Nakamura (Tokyo Medical and Dental University, Tokyo, Japan) for providing CRTH2-deficient mice.

This work was supported by the National Natural Science Foundation of China (grants 91439204, 81525004, 81790623, and 91639302), the Chinese Ministry of Science and Technology (2017YFC1307404 and 2017YFC1307402), and Postgraduate Innovation Fund of "13th Five-Year Comprehensive Investment," Tianjin Medical University (11601501/2016YJ0210). Ying Yu is a fellow at the Jiangsu Collaborative Innovation Center for Cardiovascular Disease Translational Medicine.

The authors declare no competing financial interests.

Author contributions: G. Chen performed statistical analysis; Y. Yu handled funding and supervision; G. Chen, S. Zuo, J. Tang, C. Zuo, D. Jia, Q. Liu, G. Liu, Q. Zhu, Y. Wang, J. Zhang, Y. Shen, D. Chen, P. Yuan, Z. Qin, C. Ruan, J. Ye, X.-J. Wang, Y. Zhou, P. Gao, P. Zhang, J. Liu, and Z.-C. Jing acquired the data; Y. Yu and A. Lu conceived and designed the research; G. Chen drafted the manuscript; and Y. Yu made critical revision of the manuscript for key intellectual content.

Submitted: 25 September 2017

Revised: 2 April 2018

Accepted: 17 May 2018

References

Anwar, A., G. Ruffenach, A. Mahajan, M. Eghbali, and S. Umar. 2016. Novel biomarkers for pulmonary arterial hypertension. *Respir. Res.* 17:88. <https://doi.org/10.1186/s12931-016-0396-6>

Barnes, P.J. 2018. Targeting cytokines to treat asthma and chronic obstructive pulmonary disease. *Nat. Rev. Immunol.* <https://doi.org/10.1038/s41577-018-0006-6>

Bartelds, B., R.L.E. van Loon, S. Mohaupt, H. Wijnberg, M.G. Dickinson, B. Boersma, J. Takens, M. van Albada, and R.M.F. Berger. 2012. Mast cell inhibition improves pulmonary vascular remodeling in pulmonary hypertension. *Chest* 141:651–660. <https://doi.org/10.1378/chest.11-0663>

Benza, R.L., D.P. Miller, M. Gomberg-Maitland, R.P. Frantz, A.J. Foreman, C.S. Coffey, A. Frost, R.J. Barst, D.B. Badesch, C.G. Elliott, et al. 2010. Predicting survival in pulmonary arterial hypertension: Insights from the Registry to Evaluate Early and Long-Term Pulmonary Arterial Hypertension Disease Management (REVEAL). *Circulation* 122:164–172. <https://doi.org/10.1161/CIRCULATIONAHA.109.898122>

Bigna, J.J., J.R. Nansseu, L.N. Um, S.R. Noumegni, P.S. Simé, L.N. Aminde, S. Koulla-Shiro, and J.J. Noubiap. 2016. Prevalence and incidence of

pulmonary hypertension among HIV-infected people in Africa: A systematic review and meta-analysis. *BMJ Open* 6:e011921. <https://doi.org/10.1136/bmjopen-2016-011921>

Bonelli, M., A. Savitskaya, C.W. Steiner, E. Rath, J.S. Smolen, and C. Scheinecker. 2009. Phenotypic and functional analysis of CD4⁺ CD25⁺ Foxp3⁺ T cells in patients with systemic lupus erythematosus. *J. Immunol.* 182:1689–1695. <https://doi.org/10.4049/jimmunol.182.3.1689>

Bonnet, S., S. Provencher, C. Guignabert, F. Perros, O. Bouchard, R.T. Schermuly, P.M. Hassoun, M. Rabinovitch, M.R. Nicolls, and M. Humbert. 2017. Translating research into improved patient care in pulmonary arterial hypertension. *Am. J. Respir. Crit. Care Med.* 195:583–595. <https://doi.org/10.1164/rccm.201607-1515PP>

Butrous, G., H.A. Ghofrani, and F. Grimminger. 2008. Pulmonary vascular disease in the developing world. *Circulation* 118:1758–1766. <https://doi.org/10.1161/CIRCULATIONAHA.107.727289>

Cho, W.K., C.M. Lee, M.J. Kang, Y. Huang, F.J. Giordano, P.J. Lee, T.K. Trow, R.J. Homer, W.C. Sessa, J.A. Elias, and C.G. Lee. 2013. IL-13 receptor $\alpha 2$ -arginase 2 pathway mediates IL-13-induced pulmonary hypertension. *Am. J. Physiol. Lung Cell. Mol. Physiol.* 304:L112–L124. <https://doi.org/10.1152/ajplung.00101.2012>

Ciucan, L., O. Bonneau, M. Hussey, N. Duggan, A.M. Holmes, R. Good, R. Stringer, P. Jones, N.W. Morrell, G. Jarai, et al. 2011. A novel murine model of severe pulmonary arterial hypertension. *Am. J. Respir. Crit. Care Med.* 184:1171–1182. <https://doi.org/10.1164/rccm.201103-0412OC>

Dahal, B.K., D. Kosanovic, C. Kaulen, T. Cornitescu, R. Savai, J. Hoffmann, I. Reiss, H.A. Ghofrani, N. Weissmann, W.M. Kuebler, et al. 2011. Involvement of mast cells in monocrotaline-induced pulmonary hypertension in rats. *Respir. Res.* 12:60. <https://doi.org/10.1186/1465-9921-12-60>

Daley, E., C. Emson, C. Guignabert, R. de Waal Malefyt, J. Louten, V.P. Kurup, C. Hogaboam, L. Taraseviciene-Stewart, N.F. Voelkel, M. Rabinovitch, et al. 2008. Pulmonary arterial remodeling induced by a Th2 immune response. *J. Exp. Med.* 205:361–372. <https://doi.org/10.1084/jem.20071008>

Dorfmueller, P., F. Perros, K. Balabanian, and M. Humbert. 2003. Inflammation in pulmonary arterial hypertension. *Eur. Respir. J.* 22:358–363. <https://doi.org/10.1183/09031936.03.00038903>

Flament, T., A. Bigot, B. Chaigne, H. Henique, E. Diot, and S. Marchand-Adam. 2016. Pulmonary manifestations of Sjogren's syndrome. *Eur. Respir. Rev.* 25:110–123.

Frid, M.G., J.A. Brunetti, D.L. Burke, T.C. Carpenter, N.J. Davie, J.T. Reeves, M.T. Roedersheimer, N. van Rooijen, and K.R. Stenmark. 2006. Hypoxia-induced pulmonary vascular remodeling requires recruitment of circulating mesenchymal precursors of a monocyte/macrophage lineage. *Am. J. Pathol.* 168:659–669. <https://doi.org/10.2353/ajpath.2006.050599>

Galiè, N., M. Humbert, J.L. Vachiery, S. Gibbs, I. Lang, A. Torbicki, G. Simonneau, A. Peacock, A. Vonk Noordegraaf, M. Beghetti, et al. ESC Scientific Document Group. 2016. 2015 ESC/ERS guidelines for the diagnosis and treatment of pulmonary hypertension: The Joint Task Force for the Diagnosis and Treatment of Pulmonary Hypertension of the European Society of Cardiology (ESC) and the European Respiratory Society (ERS): Endorsed by: Association for European Paediatric and Congenital Cardiology (AEPC), International Society for Heart and Lung Transplantation (ISHLT). *Eur. Heart J.* 37:67–119. <https://doi.org/10.1093/eurheartj/ehv317>

Gavilanes, F., C.J. Fernandes, and R. Souza. 2016. Pulmonary arterial hypertension in schistosomiasis. *Curr. Opin. Pulm. Med.* 22:408–414. <https://doi.org/10.1097/MCP.0000000000000300>

Germain, M., M. Eyries, D. Montani, O. Poirier, B. Girerd, P. Dorfmueller, F. Coulet, S. Nadaud, S. Maugey, C. Guignabert, et al. 2013. Genome-wide association analysis identifies a susceptibility locus for pulmonary arterial hypertension. *Nat. Genet.* 45:518–521. <https://doi.org/10.1038/ng.2581>

Graham, B.B., M.M. Mentink-Kane, H. El-Haddad, S. Purnell, L. Zhang, A. Zaiman, E.F. Redente, D.W. Riches, P.M. Hassoun, A. Bandeira, et al. 2010. Schistosomiasis-induced experimental pulmonary hypertension: Role of interleukin-13 signaling. *Am. J. Pathol.* 177:1549–1561. <https://doi.org/10.2353/ajpath.2010.100063>

Graham, B.B., J. Chabon, L. Gebreab, J. Poole, E. Debella, L. Davis, T. Tanaka, L. Sanders, N. Dropcho, A. Bandeira, et al. 2013. Transforming growth factor- β signaling promotes pulmonary hypertension caused by Schistosoma mansoni. *Circulation* 128:1354–1364. <https://doi.org/10.1161/CIRCULATIONAHA.113.003072>

Gras, D., P. Chanez, I. Vachier, A. Petit, and A. Bourdin. 2013. Bronchial epithelium as a target for innovative treatments in asthma. *Pharmacol. Ther.* 140:290–305. <https://doi.org/10.1016/j.pharmthera.2013.07.008>

- Harbaum, L., E. Renk, S. Yousef, A. Glatzel, N. Lüneburg, J.K. Hennigs, T. Oqueka, H.J. Baumann, D. Atanackovic, E. Grünig, et al. 2016. Acute effects of exercise on the inflammatory state in patients with idiopathic pulmonary arterial hypertension. *BMC Pulm. Med.* 16:145. <https://doi.org/10.1186/s12890-016-0301-6>
- Hecker, M., Z. Zaslona, G. Kwapiszewska, G. Niess, A. Zakrzewicz, E. Hergeleider, J. Wilhelm, L.M. Marsh, D. Sedding, W. Klepetko, et al. 2010. Dysregulation of the IL-13 receptor system: A novel pathomechanism in pulmonary arterial hypertension. *Am. J. Respir. Crit. Care Med.* 182:805–818. <https://doi.org/10.1164/rccm.200909-1367OC>
- Hirai, H., K. Tanaka, O. Yoshie, K. Ogawa, K. Kenmotsu, Y. Takamori, M. Ichimasa, K. Sugamura, M. Nakamura, S. Takano, and K. Nagata. 2001. Prostaglandin D₂ selectively induces chemotaxis in T helper type 2 cells, eosinophils, and basophils via seven-transmembrane receptor CRTH2. *J. Exp. Med.* 193:255–261. <https://doi.org/10.1084/jem.193.2.255>
- Ikutani, M., S. Ogawa, T. Yanagibashi, T. Nagai, K. Okada, Y. Furuichi, and K. Takatsu. 2018. Elimination of eosinophils using anti-IL-5 receptor alpha antibodies effectively suppresses IL-33-mediated pulmonary arterial hypertrophy. *Immunobiology.* 223:486–492. <https://doi.org/10.1016/j.imbio.2017.12.002>
- Ito, T., T. Okada, H. Miyashita, T. Nomoto, M. Nonaka-Sarukawa, R. Uchibori, Y. Maeda, M. Urabe, H. Mizukami, A. Kume, et al. 2007. Interleukin-10 expression mediated by an adeno-associated virus vector prevents monocrotaline-induced pulmonary arterial hypertension in rats. *Circ. Res.* 101:734–741. <https://doi.org/10.1161/CIRCRESAHA.107.153023>
- Jiang, H., M.B. Harris, and P. Rothman. 2000. IL-4/IL-13 signaling beyond JAK/STAT. *J. Allergy Clin. Immunol.* 105:1063–1070. <https://doi.org/10.1067/mai.2000.107604>
- Kherbeck, N., M.C. Tamby, G. Bussone, H. Dib, F. Perros, M. Humbert, and L. Mouthon. 2013. The role of inflammation and autoimmunity in the pathophysiology of pulmonary arterial hypertension. *Clin. Rev. Allergy Immunol.* 44:31–38. <https://doi.org/10.1007/s12016-011-8265-z>
- Kumar, R., C. Mickael, J. Chabon, L. Gebreab, A. Rutebemberwa, A.R. Garcia, D.E. Koyanagi, L. Sanders, A. Gandjeva, M.T. Kearns, et al. 2015. The causal role of IL-4 and IL-13 in Schistosoma mansoni pulmonary hypertension. *Am. J. Respir. Crit. Care Med.* 192:998–1008. <https://doi.org/10.1164/rccm.201410-1820OC>
- Li, Z., Y. Zhang, Z. Liu, X. Wu, Y. Zheng, Z. Tao, K. Mao, J. Wang, G. Lin, L. Tian, et al. 2011. ECM1 controls T(H)2 cell egress from lymph nodes through re-expression of SIP(1). *Nat. Immunol.* 12:178–185. <https://doi.org/10.1038/ni.1983>
- Lu, A., C. Zuo, Y. He, G. Chen, L. Piao, J. Zhang, B. Xiao, Y. Shen, J. Tang, D. Kong, et al. 2015. EP3 receptor deficiency attenuates pulmonary hypertension through suppression of Rho/TGF- β 1 signaling. *J. Clin. Invest.* 125:1228–1242. <https://doi.org/10.1172/JCI77656>
- Mabalarajan, U., A.K. Dinda, S. Kumar, R. Roshan, P. Gupta, S.K. Sharma, and B. Ghosh. 2008. Mitochondrial structural changes and dysfunction are associated with experimental allergic asthma. *J. Immunol.* 181:3540–3548. <https://doi.org/10.4049/jimmunol.181.5.3540>
- Marchese, A., M. Sawzdargo, T. Nguyen, R. Cheng, H.H. Heng, T. Nowak, D.S. Im, K.R. Lynch, S.R. George, and B.F. O'Dowd. 1999. Discovery of three novel orphan G-protein-coupled receptors. *Genomics.* 56:12–21. <https://doi.org/10.1006/geno.1998.5655>
- Mizuno, S., L. Farkas, A. Al Husseini, D. Farkas, J. Gomez-Arroyo, D. Kraskauskas, M.R. Nicolls, C.D. Cool, H.J. Bogaard, and N.F. Voelkel. 2012. Severe pulmonary arterial hypertension induced by SU5416 and ovalbumin immunization. *Am. J. Respir. Cell Mol. Biol.* 47:679–687. <https://doi.org/10.1165/rcmb.2012-0077OC>
- Moon, T.C., E. Campos-Alberto, T. Yoshimura, G. Bredo, A.M. Rieger, L. Puttagunta, D.R. Barreda, A.D. Befus, and L. Cameron. 2014. Expression of DP2 (CRTh2), a prostaglandin D₂ receptor, in human mast cells. *PLoS One.* 9:e108595. <https://doi.org/10.1371/journal.pone.0108595>
- Nagata, K., H. Hirai, K. Tanaka, K. Ogawa, T. Aso, K. Sugamura, M. Nakamura, and S. Takano. 1999a. CRTH2, an orphan receptor of T-helper-2-cells, is expressed on basophils and eosinophils and responds to mast cell-derived factor(s). *FEBS Lett.* 459:195–199. [https://doi.org/10.1016/S0014-5793\(99\)01251-X](https://doi.org/10.1016/S0014-5793(99)01251-X)
- Nagata, K., K. Tanaka, K. Ogawa, K. Kemmotsu, T. Imai, O. Yoshie, H. Abe, K. Tada, M. Nakamura, K. Sugamura, and S. Takano. 1999b. Selective expression of a novel surface molecule by human Th2 cells in vivo. *J. Immunol.* 162:1278–1286.
- Ober, C., and T.C. Yao. 2011. The genetics of asthma and allergic disease: A 21st century perspective. *Immunol. Rev.* 242:10–30. <https://doi.org/10.1111/j.1600-065X.2011.01029.x>
- Palikhe, N.S., C. Laratta, D. Nahirney, D. Vethanayagam, M. Bhutani, H. Vliagoffits, and L. Cameron. 2016. Elevated levels of circulating CD4(+) CRTh2(+) T cells characterize severe asthma. *Clin. Exp. Allergy.* 46:825–836.
- Park, S.H., W.C. Chen, C. Hoffman, L.M. Marsh, J. West, and G. Grunig. 2013. Modification of hemodynamic and immune responses to exposure with a weak antigen by the expression of a hypomorphic BMPR2 gene. *PLoS One.* 8:e55180. <https://doi.org/10.1371/journal.pone.0055180>
- Park, S.H., W.C. Chen, N. Esmaili, B. Lucas, L.M. Marsh, J. Reibman, and G. Grunig. 2014. Interleukin 13- and interleukin 17A-induced pulmonary hypertension phenotype due to inhalation of antigen and fine particles from air pollution. *Pulm. Circ.* 4:654–668. <https://doi.org/10.1086/678511>
- Price, L.C., S.J. Wort, F. Perros, P. Dorfmueller, A. Huertas, D. Montani, S. Cohen-Kaminsky, and M. Humbert. 2012. Inflammation in pulmonary arterial hypertension. *Chest.* 141:210–221. <https://doi.org/10.1378/chest.11-0793>
- Rabinovitch, M. 2012. Molecular pathogenesis of pulmonary arterial hypertension. *J. Clin. Invest.* 122:4306–4313. <https://doi.org/10.1172/JCI60658>
- Rabinovitch, M., C. Guignabert, M. Humbert, and M.R. Nicolls. 2014. Inflammation and immunity in the pathogenesis of pulmonary arterial hypertension. *Circ. Res.* 115:165–175. <https://doi.org/10.1161/CIRCRESAHA.113.301141>
- Radstake, T.R., L. van Bon, J. Broen, M. Wenink, K. Santegoets, Y. Deng, A. Hussaini, R. Simms, W.W. Cruikshank, and R. Lafyatis. 2009. Increased frequency and compromised function of T regulatory cells in systemic sclerosis (SSc) is related to a diminished CD69 and TGFbeta expression. *PLoS One.* 4:e5981. <https://doi.org/10.1371/journal.pone.0005981>
- Rael, E.L., and R.F. Lockey. 2011. Interleukin-13 signaling and its role in asthma. *World Allergy Organ. J.* 4:54–64. <https://doi.org/10.1097/WOX.0b013e31821188e0>
- Rydell-Törmänen, K., J.R. Johnson, R. Fattouh, M. Jordana, and J.S. Erjefält. 2008a. Induction of vascular remodeling in the lung by chronic house dust mite exposure. *Am. J. Respir. Cell Mol. Biol.* 39:61–67. <https://doi.org/10.1165/rcmb.2007-0441OC>
- Rydell-Törmänen, K., L. Uller, and J.S. Erjefält. 2008b. Remodeling of extra-bronchial lung vasculature following allergic airway inflammation. *Respir. Res.* 9:18. <https://doi.org/10.1186/1465-9921-9-18>
- Said, S.I., S.A. Hamidi, K.G. Dickman, A.M. Szema, S. Lyubsky, R.Z. Lin, Y.P. Jiang, J.J. Chen, J.A. Waschek, and S. Kort. 2007. Moderate pulmonary arterial hypertension in male mice lacking the vasoactive intestinal peptide gene. *Circulation.* 115:1260–1268.
- Said, S.I., S.A. Hamidi, and L. Gonzalez Bosc. 2010. Asthma and pulmonary arterial hypertension: Do they share a key mechanism of pathogenesis? *Eur. Respir. J.* 35:730–734. <https://doi.org/10.1183/09031936.00097109>
- Savai, R., S.S. Pullamsetti, J. Kolbe, E. Bieniek, R. Voswinckel, L. Fink, A. Scheed, C. Ritter, B.K. Dahal, A. Vater, et al. 2012. Immune and inflammatory cell involvement in the pathology of idiopathic pulmonary arterial hypertension. *Am. J. Respir. Crit. Care Med.* 186:897–908. <https://doi.org/10.1164/rccm.201202-0335OC>
- Schmidt, J.A., F.M. Bell, E. Akam, C. Marshall, I.A. Dainty, A. Heinemann, I.G. Dougall, R.V. Bonnert, and C.A. Sargent. 2013. Biochemical and pharmacological characterization of AZD1981, an orally available selective DP2 antagonist in clinical development for asthma. *Br. J. Pharmacol.* 168:1626–1638. <https://doi.org/10.1111/bph.12053>
- Shi, M., G. Shi, J. Tang, D. Kong, Y. Bao, B. Xiao, C. Zuo, T. Wang, Q. Wang, Y. Shen, et al. 2014. Myeloid-derived suppressor cell function is diminished in aspirin-triggered allergic airway hyperresponsiveness in mice. *J. Allergy Clin. Immunol.* 134:1163–1174.
- Spik, I., C. Brénuchon, V. Angéli, D. Staumont, S. Fleury, M. Capron, F. Trottein, and D. Dombrowicz. 2005. Activation of the prostaglandin D2 receptor DP2/CRTH2 increases allergic inflammation in mouse. *J. Immunol.* 174:3703–3708. <https://doi.org/10.4049/jimmunol.174.6.3703>
- Stacher, E., B.B. Graham, J.M. Hunt, A. Gandjeva, S.D. Groshong, V.V. McLaughlin, M. Jessup, W.E. Grizzle, M.A. Aldred, C.D. Cool, and R.M. Tuder. 2012. Modern age pathology of pulmonary arterial hypertension. *Am. J. Respir. Crit. Care Med.* 186:261–272. <https://doi.org/10.1164/rccm.201201-0164OC>
- Szema, A.M., S.A. Hamidi, S. Lyubsky, K.G. Dickman, S. Mathew, T. Abdel-Razek, J.J. Chen, J.A. Waschek, and S.I. Said. 2006. Mice lacking the VIP gene show airway hyperresponsiveness and airway inflammation, partially reversible by VIP. *Am. J. Physiol. Lung Cell. Mol. Physiol.* 291:L880–L886. <https://doi.org/10.1152/ajplung.00499.2005>
- Thiriou, D., I. Morianos, G. Xanthou, and K. Samitas. 2017. Innate immunity as the orchestrator of allergic airway inflammation and resolution in

- asthma. *Int. Immunopharmacol.* 48:43–54. <https://doi.org/10.1016/j.intimp.2017.04.027>
- Voelkel, N.F., R. Tamosiuniene, and M.R. Nicolls. 2016. Challenges and opportunities in treating inflammation associated with pulmonary hypertension. *Expert Rev. Cardiovasc. Ther.* 14:939–951. <https://doi.org/10.1080/14779072.2016.1180976>
- Wang, Z., R.S. Lakes, M. Golob, J.C. Eickhoff, and N.C. Chesler. 2013. Changes in large pulmonary arterial viscoelasticity in chronic pulmonary hypertension. *PLoS One.* 8:e78569. <https://doi.org/10.1371/journal.pone.0078569>
- Wei, L.H., A.T. Jacobs, S.M. Morris Jr., and L.J. Ignarro. 2000. IL-4 and IL-13 upregulate arginase I expression by cAMP and JAK/STAT6 pathways in vascular smooth muscle cells. *Am. J. Physiol. Cell Physiol.* 279:C248–C256. <https://doi.org/10.1152/ajpcell.2000.279.1.C248>
- Weisel, F.C., C. Kloeping, A. Pichl, A. Sydykov, B. Kojonazarov, J. Wilhelm, M. Roth, K.M. Ridge, K. Igarashi, K. Nishimura, et al. 2014. Impact of S-adenosylmethionine decarboxylase 1 on pulmonary vascular remodeling. *Circulation.* 129:1510–1523. <https://doi.org/10.1161/CIRCULATIONAHA.113.006402>
- Weng, M., D.M. Baron, K.D. Bloch, A.D. Luster, J.J. Lee, and B.D. Medoff. 2011. Eosinophils are necessary for pulmonary arterial remodeling in a mouse model of eosinophilic inflammation-induced pulmonary hypertension. *Am. J. Physiol. Lung Cell. Mol. Physiol.* 301:L927–L936. <https://doi.org/10.1152/ajplung.00049.2011>
- Wojno, E.D., L.A. Monticelli, S.V. Tran, T. Alenghat, L.C. Osborne, J.J. Thome, C. Willis, A. Budelsky, D.L. Farber, and D. Artis. 2015. The prostaglandin D₂ receptor CRTH2 regulates accumulation of group 2 innate lymphoid cells in the inflamed lung. *Mucosal Immunol.* 8:1313–1323. <https://doi.org/10.1038/mi.2015.21>
- Xue, L., S.L. Gyles, F.R. Wettley, L. Gazi, E. Townsend, M.G. Hunter, and R. Pettipher. 2005. Prostaglandin D₂ causes preferential induction of proinflammatory Th2 cytokine production through an action on chemoattractant receptor-like molecule expressed on Th2 cells. *J. Immunol.* 175:6531–6536. <https://doi.org/10.4049/jimmunol.175.10.6531>
- Xue, L., A. Barrow, and R. Pettipher. 2009. Interaction between prostaglandin D and chemoattractant receptor-homologous molecule expressed on Th2 cells mediates cytokine production by Th2 lymphocytes in response to activated mast cells. *Clin. Exp. Immunol.* 156:126–133. <https://doi.org/10.1111/j.1365-2249.2008.03871.x>
- Yamaji-Kegan, K., E. Takimoto, A. Zhang, N.C. Weiner, L.W. Meuchel, A.E. Berger, C. Cheadle, and R.A. Johns. 2014. Hypoxia-induced mitogenic factor (FIZZ1/RELM α) induces endothelial cell apoptosis and subsequent interleukin-4-dependent pulmonary hypertension. *Am. J. Physiol. Lung Cell. Mol. Physiol.* 306:L1090–L1103. <https://doi.org/10.1152/ajplung.00279.2013>
- Yang, G., L. Li, A. Volk, E. Emmell, T. Petley, J. Giles-Komar, P. Rafferty, M. Lakshminarayanan, D.E. Griswold, P.J. Bugelski, and A.M. Das. 2005. Therapeutic dosing with anti-interleukin-13 monoclonal antibody inhibits asthma progression in mice. *J. Pharmacol. Exp. Ther.* 313:8–15. <https://doi.org/10.1124/jpet.104.076133>
- Yang, Q., M. Shi, Y. Shen, Y. Cao, S. Zuo, C. Zuo, H. Zhang, D.I. Gabrilovich, Y. Yu, and J. Zhou. 2014. COX-1-derived thromboxane A₂ plays an essential role in early B-cell development via regulation of JAK/STAT5 signaling in mouse. *Blood.* 124:1610–1621. <https://doi.org/10.1182/blood-2014-03-559658>
- Yeager, M.E., C.M. Nguyen, D.D. Belchenko, K.L. Colvin, S. Takatsuki, D.D. Ivy, and K.R. Stenmark. 2012. Circulating myeloid-derived suppressor cells are increased and activated in pulmonary hypertension. *Chest.* 141:944–952. <https://doi.org/10.1378/chest.11-0205>
- Zhao, F., Y. Zhang, H. Wang, M. Jin, S. He, Y. Shi, Y. Guo, and Y. Zhang. 2011. Blockade of osteopontin reduces alloreactive CD8⁺ T cell-mediated graft-versus-host disease. *Blood.* 117:1723–1733. <https://doi.org/10.1182/blood-2010-04-281659>